LABORATORI NAZIONALI DI FRASCATI
SIS – Pubblicazioni

LNF–02/016 (P)
12 Luglio 2002

Papers presented at EPAC 2002

Accelerator Division

Contributions to the
8th European Particle Accelerator Conference (EPAC 2002)
La Villette – Paris, 3 – 7 June 2002

CONTENTS

N.T.A. – NF

N.T.A. – SPARC-X:

LONGITUDINAL QUADRUPOLE INSTABILITY IN DAΦNE ELECTRON RING

A. Drago, A. Gallo, A. Ghigo, M. Zobov, INFN-LNF, Frascati, Italy

Abstract

A longitudinal quadrupole (q-pole) instability was limiting the maximum stable current in the DAΦNE e- ring at ~800mA. The instability threshold dependence on various machine parameters as radiofrequency voltage (Vrf) and momentum compaction has been measured. An unexpected interaction with the longitudinal feedback system has been found and the understanding of a damping mechanism has allowed increasing the threshold. The maximum stable beam total current has now reached more then 1.85A, no longer limited by the quadrupole instability.

1 INTRODUCTION

DAΦNE is a Φ–factory, e+/e- collider in operation for physics experiments since 1999 with gradually increasing peak and integrated luminosities [1]. In order to reach the high required luminosity, in the $10^{32}cm^{-2}sec^{-1}$ range, multibunch beams with currents of several Amperes have to stored in both rings of the collider. The design current per single bunch of 44mA has been successfully exceeded in both rings. About 200mA have been stored in a single bunch without destroying instabilities. In the multibunch operation, a longitudinal quadrupole (q-pole) instability was limiting the maximum stable current in DAΦNE e- ring to ~800mA. The experimental study of the instability has allowed to find measures to damp or avoid it and to store stable e- beam with more then 1.85A. Below we discuss the instability phenomenology, its threshold dependence on different machine parameters, describe the cure and propose possible directions for further study of the instability mechanism.

2 QUADRUPOLE INSTABILITY

Considering the longitudinal dynamics in DAΦNE, strong, coupled bunch synchrotron oscillations make active damping systems necessary.

In each main ring, a broadband bunch-by-bunch longitudinal feedback (LFB) is operating since 1998. This system has been developed in collaboration with PEP-II/SLAC and ALS/Berkeley [2]. A zero-mode feedback, acting around the RF cavity is also operating.

These systems work fairly well, but last year an unexpected longitudinal quadrupole instability was limiting the total current to ~800mA in the e- ring. This trouble appeared usually above 600mA, producing harmful effects for the beam-beam interaction.

2.1 Phenomenon Description

To introduce the argument, let's consider, as an example, a rather usual case of 45 stored e- bunch, each followed by one empty bucket, with less than 300mA of total beam current, Vrf = 120kV. With longitudinal feedback on, no sidebands are visible around the n-th revolution harmonic, see Fig. 1.

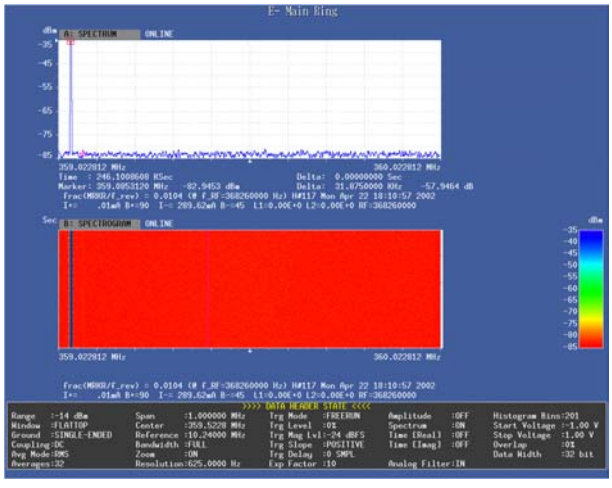

Figure 1: Multibunch beam spectrum with LFB on.

Considering now the same case with LFB off, it is possible to observe several sidebands indicating large dipolar oscillations (see Fig. 2).

The difference between the first sideband and the revolution harmonic is equal to the synchrotron frequency (dipole), the other satellite oscillations are multiple of the first one.

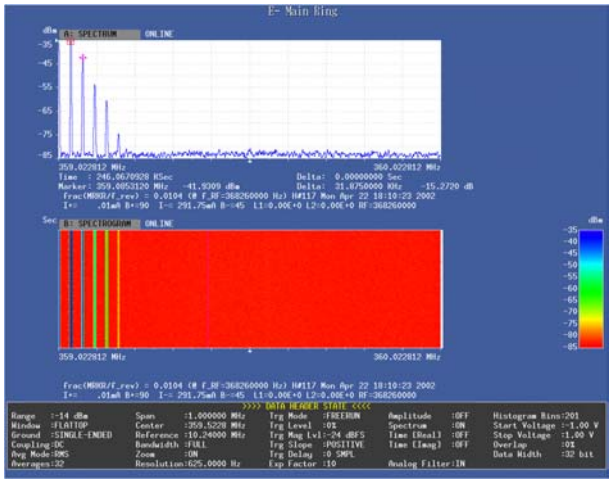

Figure 2: Multibunch beam spectrum with LFB off.

Still, in multibunch mode with LFB on, at high currents (between 600 and 800mA), and only in the electron main ring a quadrupole line (without dipole) appeared, limiting further current injection, as seen in Fig. 3, indicated by the cursor.

The current limit consists of the fact that new injections can produce loss of bunches and/or loss of LFB control with successive large decrease of the total beam current.

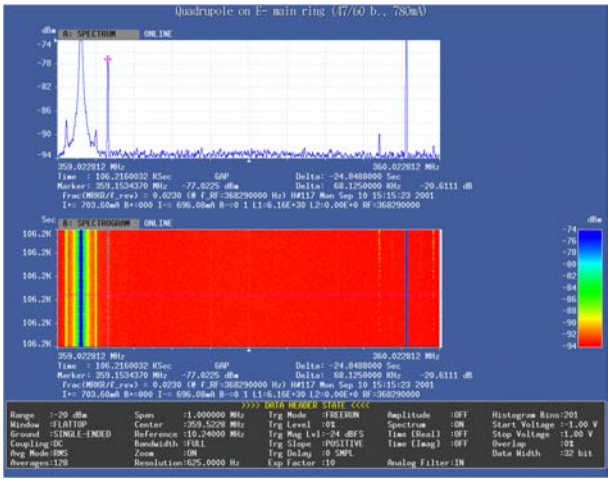

Figure 3: Quadrupole instability in e- ring at ~700mA with LFB on (Vrf=170kV).

The current limit consists of the fact that new injections can produce loss of bunches and/or loss of LFB control with successive large decrease of the total beam current.

Besides, there is another peculiar aspect: considering for example a multibunch case with Vrf=120kV, 770 mA, 45/60 bunches, it is possible to observe the q-pole frequency at 58.75kHz, while the second harmonic of the synchrotron frequency is at 60kHz, with a difference of -1.25kHz from the zero current line.

2.2 Relevant Parameters

In order to overcome the current limit, the q-pole instability threshold has been measured as a function of the following machine parameters:

- Radiofrequency voltage
- Momentum compaction (α_c)
- Orbit (considering the eventuality of a trapped mode)
- Injected patterns and number of bunches
- Bunch length and LFB backend setup.

2.3 First Measurements

A clear variation of the q-pole threshold was observed as function of the RF voltage: with 47 bunches the threshold was ~550mA with Vrf =120kV and ~750mA with Vrf =170kV.

The dependence on momentum compaction has been evaluated. A ~10% increase of the α_c value (from .03 to .033) has allowed to increase the quadrupole threshold by ~ 17% (from ~750 to ~880mA in 47 bunches) (Oct. 2001). However, variations of this parameter have not given a definitive solution for the instability damping.

Afterwards the q-pole threshold has been measured varying number of bunch and fill patterns. It has been found that the threshold increases with the number of bunches, but this is neither conclusive nor sufficient to cancel the current limit.

2.4 Two Different Behaviours

The measurement that has indicated more clearly the way to follow, was that of single bunch q-pole threshold versus RF voltage, with LFB off and on, see Fig.4.

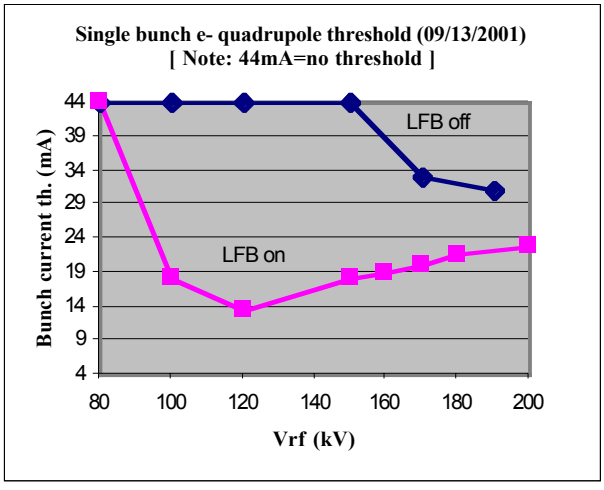

Figure 4: Single Bunch Q-pole Threshold.

Comparison shows that the lowest threshold case with LFB on corresponds to no q-pole evidence with LFB off. In general, the two situations (with and without LFB) have different behaviour as if they were two different types of quadrupole instabilities at all. This persuasion has led to study any possible interaction between LFB and q-pole instability threshold.

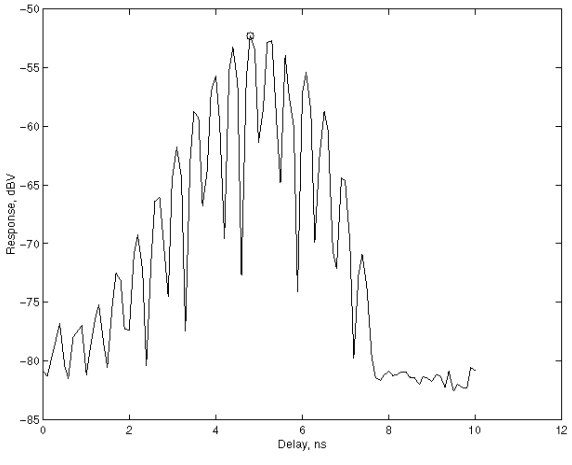

Figure 5: Longitudinal backend response.

2.5 Bunch Length and LFB backend (BE)

Figure 5 shows the single bunch longitudinal backend response as a function of timing in the cavity kicker of the LFB system. The bunch passage should be synchronized with the centre of the highest lobe to exploit the most of the power. The useful period is 418psec and contiguous lobes are in LFB opposite phases.

On the other hand, the measured e- bunch length (FWHM) is <144psec at 1mA and grows up to 300psec at 39mA, with Vrf equal to 120kV [3] (see Fig. 6).

Measuring FWHM versus Vrf, bunch length decreases as the voltage increases.

From these data, it can be supposable that a bunch length comparable to the BE period could drive an interaction between LFB and q-pole instability.

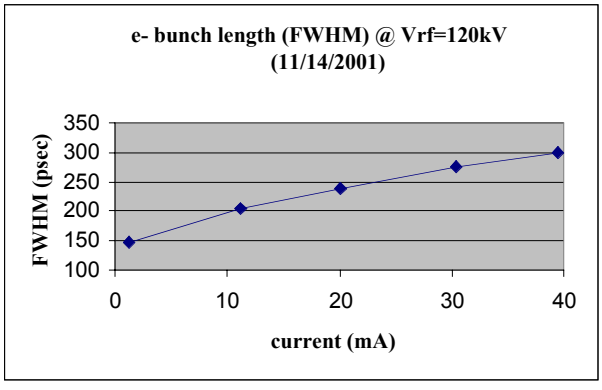

Figure 6: Bunch length versus bunch current.

2.6 Q-pole with LFB off

Now we consider the case of q-pole oscillations with LFB off, in single bunch, with Vrf=190kV: it is a RF voltage higher than the used one and q-pole appears above 24mA. In this case, after turning on LFB, we have observed that the BE delay shift does not show effects. Still, increasing by 256 times the LFB gain, the q-pole sideband is attenuated and shifted. This lets us think that it is truly an effect of the LFB.

3 THE CURE

Measuring the q-pole threshold versus LFB backend delay, we have found that increasing conveniently the BE timing (i.e. kicking the bunch tail) produces higher or no thresholds and decreasing delay (i.e. kicking the bunch head) lowers q-pole threshold.

Still, in single bunch with Vrf=120kV and beam current > 26mA, just decreasing by 150psec the LFB backend delay, it is possible to excite a quadrupole motion (note that this happens also in the e+ ring at higher currents).

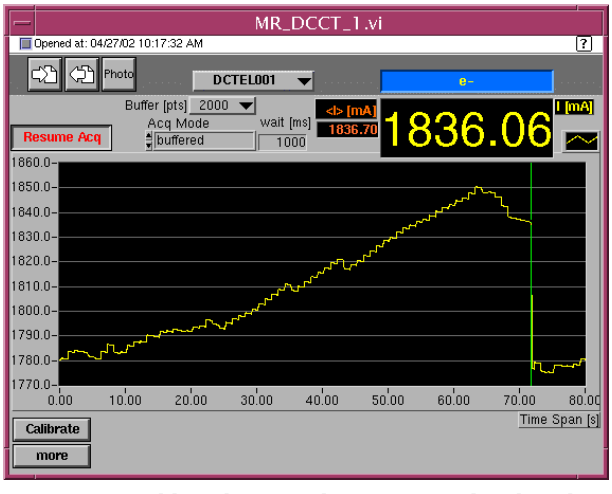

Figure 7: A stable e- beam with 1850mA and 90 bunches.

After this discovery, it has been always possible to adjust the LFB backend delay to avoid q-pole instability for all the typical collision cases and store more then 1850mA of stable electron beam in April 2002 (see Fig. 7).

4 DISCUSSION AND DEVELOPMENTS

Despite the cure found experimentally is very reliable, the underlying mechanism(s) still has to be explained.

In the future, it would be interesting to study more deeply the phenomenon. To do this, some working directions could be outlined:

a) Use a narrower LFB bandpass filter. In fact, e- LFB uses a 40.5kHz centered FIR filter that has a good –90 degree phase response for the dipole. This is enough convenient to damp it and to coexist with the mode zero oscillations, but the filter phase response could be critical at the longitudinal quadrupole frequency and narrower band filters would have lower amplitude responses for the q-pole (purely software solution).

b) Try a lower frequency as LFB BE carrier. If 11/4*RF would be used in place of 13/4*RF the BE period would increase by 80psec (expensive solution in term of hardware and machine time, probably).

c) Develop a LFB setup for the case in par.2.6.

d) Create numerical models and perform simulation of the instability including LFB.

5 CONCLUSIONS

After discovering how to manage q-pole motion, it has been possible to exceed the 800mA limit in collision. To use correctly the LFB, the trade-off between dipole and q-pole responses has to be carefully checked. During 2002, DAΦNE no longer suffered longitudinal q-pole limits. To put in collision 2 Amperes e- beam against a 2 Amperes e+ beam is the possible next development.

6 ACKNOWLEDGEMENTS

Thanks to A. Hoffman, J.D.Fox and D.Teytelman for an interesting even though informal meeting held in last December at SLAC. Shyam Prabhakar has suggested modifying the bunch pattern and has kindly provided a software tool to calculate the effects. Thanks to M. Serio for many discussions.

7 REFERENCES

[1] M. Zobov *et al.*, “Luminosity Performance of DAΦNE”, this conference, MOPRI007.

[2] J.D. Fox *et al.*, “Programmable DSP Based Multibunch Feedback: Operational Experience from Six Installations", SLAC-PUB-8410, May 2000. BIW 2000, Cambridge, Mass., May 2000.

[3] A. Ghigo *et al.*, “DAΦNE Broadband Impedance”, this conference, WEPRI025.

LUMINOSITY PERFORMANCE OF DAΦNE

M. Zobov, D. Alesini, G. Benedetti, S. Bertolucci, M.E. Biagini, C. Biscari, R. Boni, M. Boscolo, A. Clozza, G. Delle Monache, G. Di Pirro, A. Drago, A. Gallo, A. Ghigo, S. Guiducci, F. Marcellini, G. Mazzitelli, C. Milardi, L. Pellegrino, M.A. Preger, P. Raimondi, R. Ricci, C. Sanelli, F. Sannibale, M. Serio, F. Sgamma, A. Stecchi, A. Stella, C. Vaccarezza, M. Vescovi, LNF-INFN, Frascati, Italy

Abstract

Since the last EPAC2000 Conference, both the peak and integrated luminosity of the e^+e^- collider DAΦNE, Italian Φ–factory, have grown by an order of magnitude. In this paper we describe the steps that have led to the luminosity increase and discuss our plans for further luminosity upgrade.

1 INTRODUCTION

The Φ–factory DAΦNE is an e^+e^- collider designed to provide luminosity in the order of 10^{32} $cm^{-2}s^{-1}$ at the energy of the Φ–resonance (1020 MeV in the centre of mass) [1]. The first experimental detector KLOE [2], aimed at the study of for CP violation, was installed in the Interaction Region 1 (IR1) of DAΦNE in March 1999. Since then DAΦNE alternates machine study and physics data taking shifts. Later, another experiment DEAR [3], for exotic atoms studies, was installed in the second interaction region (IR2). The peak luminosity growth in time for the KLOE experiment is shown in Fig. 1.

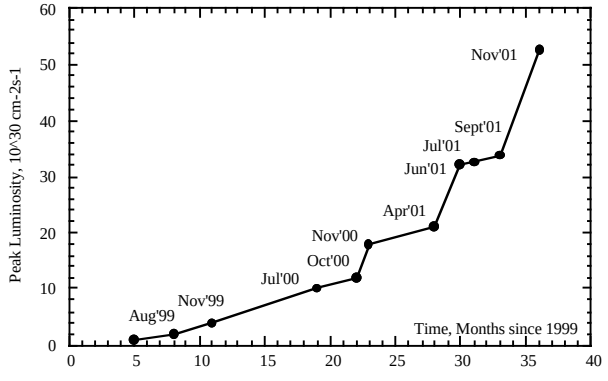

Figure 1: DAΦNE peak luminosity.

The peak luminosity was increased by more than a factor of 10 during the past two years (from November 1999 to November 2001) reaching a maximum value of 5.2 10^{31} $cm^{-2}s^{-1}$. As shown in Figure 2, during last year the peak luminosity is steadily increasing, while the integrated luminosity per day grows faster, indicating an improvement of the overall efficiency and at present its peak value is 3 pb^{-1}/day. About 200 pb^{-1} have been logged by the KLOE experiment. December 2001 and 3 months after a shut down in January/February 2002 were dedicated to the collider tuning and data taking for the DEAR experiment. The experience gained with the KLOE lattice helped in reaching practically the same luminosity of 5.0 10^{31} $cm^{-2}s^{-1}$ at IR2 in a short time and to substantially reduce the background that was of a crucial importance for the DEAR experiment. About 20 pb^{-1} were logged by this experiment and, due to both machine and detector improvements, the signal-to-noise ratio has been enhanced by a factor of 40 with respect to the DEAR shifts in May 2001. An important contribution to the background reduction came from the decrease of the horizontal beta function at the interaction point.

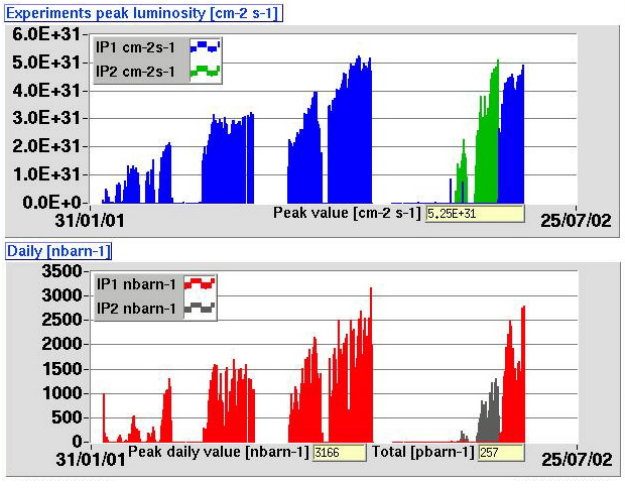

Figure 2: DAΦNE peak and daily integrated luminosity.

In May 2002 data taking shifts for KLOE resumed with slightly lower luminosity, but with a background reduction by a factor 3 with respect to December. In this paper we describe our experience on the DAΦNE luminosity performance optimisation and discuss our future plans.

2 LUMINOSITY OPTIMISATION

The above described significant luminosity progress was realized by means of continuous machine physics study. The major items leading to the luminosity performance improvement can be summarised as follows:

- Working point choice.
- Coupling correction.
- Nonlinear beam dynamics study.
- Linear optics improvements.
- Single- and multibunch instability cures.
- Collider parameters fine tuning during data taking.

A dedicated work on background reduction including orbits and optical functions correction, working point fine

tuning, sextupole strengths and scraper positions optimisation allowed to operate the collider in the "topping up" mode without switching off the KLOE drift chamber during injection. This resulted in a significant average and daily integrated luminosity increase.

2.1 Working Point Choice

Analytical estimates and numerical simulations [4] have shown that the only working point on the tune diagram above integers, where the project luminosity parameters with $\xi_x = \xi_y = 0.04$ can be met, is a small area around (ΔQ_x=0.09, ΔQ_y=0.07). However, during collider commissioning the working point (0.15; 0.21) was chosen for collisions. Despite some expected reduction in luminosity, this point has a number of advantages with respect to (0.09; 0.07), of particular importance during machine tuning: the dynamic aperture is larger, the second order chromaticity terms are smaller, coupling correction is easier, the closed orbit is less sensitive to magnetic element errors and so on. An intensive numerical study has been carried out for this working point [5], considering different factors affecting the luminosity performance such as the separation at the second interaction point, vertical crossing angle, parasitic crossings and others. At present the positron ring is tuned at this working point. Instead, we had to shift the electron ring working point from (0.15; 0.21). There are two main reasons for that:

- Performing the tune scan it was found that the lifetime for this working point was low even without beam-beam collisions. This was attributed to nonlinear lattice resonances.
- At high currents a strong vertical instability in the e+ ring is transmitted to the e- ring if the tunes are equal. Separating the tunes the instability is eliminated by the Landau damping due to the nonlinear beam-beam interaction.

Experimentally, after gradual optimisation of collision parameters, the working point of the electron ring was set to (0.11; 0.14). Actually, according to numerical simulations this is yet another "safe" working point in the tune area above integers where the beam blow up is relatively small and tails induced by the beam-beam interaction are well confined within the dynamic aperture.

2.2 Coupling Correction

In a storage ring different sources can excite coupling between vertical and horizontal betatron oscillations: skew magnets, vertical dispersion, solenoids, off-axis sextupoles etc. Depending on the coupling sources and their distribution along the ring, the normal betatron modes can propagate in a different way down to the interaction point (IP). As a consequence, the two beams can have different sizes and rotations at the IP resulting in different core blow up and tail growth. Numerical simulations have shown that for the nominal coupling of 1% the beam core blow up in DAΦNE may vary in a wide range. This was a clear indication of the necessity of deeper coupling study and correction below the design value. Details of this work are described elsewhere [6]. Here we list the main steps that led to coupling reduction:

- KLOE detector solenoid and compensator magnet current variation
- Global coupling correction with skew quadrupoles.
- Residual vertical dispersion correction.
- Nonlinear terms minimization.
- Working point fine tuning.

As a result, coupling was reduced down to 0.2% for both rings and the luminosity in single bunch collisions increased by, at least, a factor of 2.

2.3 Nonlinear Dynamics Study

Nonlinear dynamics study was considered as a crucial task for luminosity increase. Three main techniques were adopted for this study: tune scans, localized orbit bumps inside critical magnetic elements and beam decoherence measurements. The tune scan was used to define safe areas for beam-beam collisions on the tune diagram not affected by nonlinear lattice resonances. By changing the tunes we observed the lifetime and blow up of a single bunch at the synchrotron light monitor. We found that for some tunes the lifetime was strongly reduced or the beam size increased. By analyzing the results we found that nonlinear resonances up to 6^{th} order were responsible for these effects. Since such resonances can be driven only by strong nonlinear magnetic elements, dedicated orbit bumps were performed and tune shifts versus bump amplitude were measured in order to recognize such elements. In particular, it was found that the wigglers are a strong source of octupole-like terms providing a cubic nonlinearity [7]. By means of a dynamic tracking system [8] we performe beam decoherence measurements and estimate directly the coefficient c_{11} of the horizontal tune shift versus amplitude. Numerical simulations carried out taking into account the measured cubic nonlinearity have shown that they have a dramatic impact on the collider luminosity performance [9]. Beam blow up and tails growth could be observed in the simulations if the coefficient $|c_{11}|$ characterizing the cubic nonlinearity exceeded 2 10^2 m^{-1}. This limit should be compared to the measured value for some lattice configurations as high as 6 10^2 m^{-1}. In the multibunch regime the maximum achievable luminosity is mainly limited by the combined effect of parasitic crossings and nonlinearities.

Experimentally, a strong correlation between the luminosity and the measured cubic nonlinearity was observed. Indeed, the present peak luminosity of 5.2 10^{31} $cm^{-2}s^{-1}$ was obtained when $|c_{11}|$ was reduced below 2 10^2 m^{-1} in both rings. In this case the luminosity scales linearly with the number of bunches.

2.4 Lattice Improvements

An important step leading to luminosity increase was obtained for KLOE by means of a new "detuned" lattice without low beta insertion at the second interaction point [10] where the beams are separated during KLOE runs.

The main advantages of this lattice can be summarised as following:

- The separation of the beams at the second IP is be larger; therefore the second IP has no influence on luminosity.
- The low beta insertion at the second IP has been eliminated thus reducing the chromaticity. This allowed to reduce β_y at the KLOE IP keeping the same sextupole strengths. β_y has been reduced from .06 m to .03 m.
- The beta functions in the wigglers are lower. As a consequence, the lattice is less sensitive to the cubic nonlinearity in comparison with the "old" KLOE lattice.

In the DEAR case the situation is worse, since the permanent magnet KLOE quadrupoles do not allow to eliminate the low β in KLOE interaction region. At the KLOE IP a β_y =.07 m has been realized, while at the DEAR IP the value of β_y is .03 m. Switching off the couple of quads nearest to the IP allowed to decrease also β_x at the IP from 4 m to 1.5 m, with a significant reduction of chromaticity and background in the experiment and luminosity improvement.

2.5 Instabilities

Stable high current multibunch beams are necessary to reach high luminosity. At present the single bunch design current of 44 mA (in interaction) has been largely exceeded. About 200 mA were stored in a non interacting single bunch in both rings without observing harmful instabilities. In the multibunch regime more than 2 A were accumulated in the electron storage ring and about 1.3 A in the positron one. Details of the high current beam dynamics are presented at this Conference [11, 12].

3 LUMINOSITY UPGRADE PLANS

Analysis of numerical simulations and experimental data together with the experience acquired during commissioning provide us with guidelines for future luminosity upgrade. In particular, the following steps will be undertaken in the near future:

- Change of the e- beam working point. Strong-strong beam-beam simulations show that the luminosity can increase by almost a factor of 2 by shifting the electron beam tune to the working point (0.15; 021). This can be done if the problem of the low lifetime for this working point in the e- ring is solved and the vertical instability is effectively damped.
- Increase of the number of bunches by filling each RF bucket. The problem of parasitic crossings (PC) in this case can be solved by increasing the separation at the PCs in terms of the horizontal beam size by providing larger horizontal crossing angle, reducing the horizontal beta function at the PC positions and decreasing the horizontal emittance. The first attempt to work with 90 consecutive bunches in the DEAR lattice has been successfully made [13].
- Further current increase both in single bunches and in multibunch beams. Deeper beam dynamics study and elimination of instability sources will accomplish this task.
- Theoretical and experimental study of nonlinear optics with recently installed octupole magnets. The octupoles give a possibility to vary the cubic nonlinearity in a wide range thus affecting beam-beam interaction. Background, dynamic aperture and lifetime improvements are also expected [14].
- Measurement and correction of the nonlinear magnetic terms on a new wiggler prototype by means of pole shimming. By applying the correction to all wigglers, the contribution to the lattice non linearity will be strongly reduced.
- Installation of a new interaction region for KLOE(IR) providing independent rotation of the permanent magnet quadrupoles. Transformation of the present triplet structure into a doublet with the goal of reducing β_x at the IP and chromaticity. Insertion of masks for backgrounds reduction is also foreseen. We expect better coupling correction within the IR and the possibility of colliding at the second IP with the KLOE solenoid off.

REFERENCES

[1] G. Vignola, "DAΦNE, The Frascati Φ-Factory," PAC'93, Washington, 1993.

[2] The KLOE Collaboration, "KLOE: a General Purpose Detector for DAΦNE", LNF-92/019 (IR), April 1992.

[3] The DEAR Collaboration, "The DEAR Case", Riv. Del Nuovo Cimento, Vol. 22, No. 11, p. 1 (1999).

[4] K. Hirata, M. Zobov, "Beam-Beam Interaction Study for DAΦNE", EPAC'96, Sitges, Spain, 1996.

[5] M. Zobov, M. Boscolo, D. Shatilov, "Beam-Beam Interaction at the Working Point (0.15; 0.21)", DAΦNE Technical Note: G-51. Frascati, March 3, 2002.

[6] C. Milardi et. al., "Optics Measurements in DAΦNE", EPAC2000, Vienna, Austria, 2000.

[7] C. Milardi et. al., "Effects of Nonlinear Terms in the Wiggler Magnets at DAΦNE", PAC'01, Chicago, USA, 2001.

[8] A. Drago, A. Stella, "Dynamic Tracking Acquisition System for DAΦNE Collider", DIPAC2001, Grenoble, France, 2001.

[9] M. Zobov, "Crosstalk between Beam-Beam Effects and Lattice Nonlineariries in DAΦNE", DAΦNE Technical Note: G-57. Frascati, July 10, 2001.

[10] C. Biscari, "Detuned Lattice for DAΦNE Main Rings", DAΦNE Technical Note: L-32. Frascati, March 1, 2001.

[11] A. Ghigo et. al., this conference.

[12] A Drago et. al., this conference.

[13] C. Biscari et. al., "Half β_x at IP2," DAΦNE Technical Note: BM-9. Frascati, April 11, 2002.

[14] C. Vaccarezza et. al., this conference.

DAΦNE CRYOGENIC COOLING SYSTEM: STATUS AND PERSPECTIVES

C. Ligi, G. Delle Monache, R. Ricci, C. Sanelli, INFN-LNF, Frascati (Rome), Italy

Abstract

The cryogenic system of DAΦNE has been continuously operating for 5 years with only few weeks of shut down per year, due to scheduled maintenance or faults. The paper describes the system and its status, along with a detailed fault analysis. The upgrades undertaken to increase the reliability of the entire system and the work to accommodate the second big DAΦNE experiment are also presented.

1 INTRODUCTION

In the original layout of the DAΦNE storage rings the cryogenic plant was needed for the cooling of several superconducting magnets. Subsequently there was an evolution in the status of the plant, both for the accelerator and for the cryogenic plant developments.

The main components of the plant are listed in the next sections, together with a description of the cooling process of the magnets. Then, all the faults related to the cryogenic plant since the year 2000 are taken into account, in order to investigate the plant performance in relation with DAΦNE operation. The future upgrades of the plant, needed to reach the final configuration, are also mentioned.

2 CRYOGENIC PLANT

The main experiments in the DAΦNE storage rings are KLOE and FINUDA, which exploit the longitudinal field of two large superconducting solenoid magnets.

Both magnets are cooled by a 4.5 K liquid Helium refrigeration system.

The layout of the cryogenic plant is shown in Fig. 1. The main components of the system are:

1) Helium Process Compressor, a KAESER FSB440 screw air compressor adapted for working with Helium. It compresses the warm gas (300 K) from ≈1.02 to ≈14 bar (max).

2) Helium Buffer Volumes, in which the low pressure gas before entering the compressor is stored. It consists of two steel cylinders of 34 m^3 each, working at a pressure between 1 and 13 bar.

3) Warm Transfer Lines, a couple of Stainless Steel seamless pipes which drive the high pressure (HP) gas from the compressor to the Cold Box and the low pressure (LP) gas from the Cold Box back to the compressor.

4) Cold Box, a LINDE TCF50 standard refrigeration system with few adaptations (see later). It has the following cryogenic capacities:

Liquefaction rate:	1.14 g/s
Refr. Capacity @ 4.45 K, 1.22bar	99 W
Refr. Capacity @ ~ 70 K	800 W

5) Cryogenic Transfer Lines, for the gas transport between the Cold Box (which is placed outside the DAΦNE hall) and the magnets.

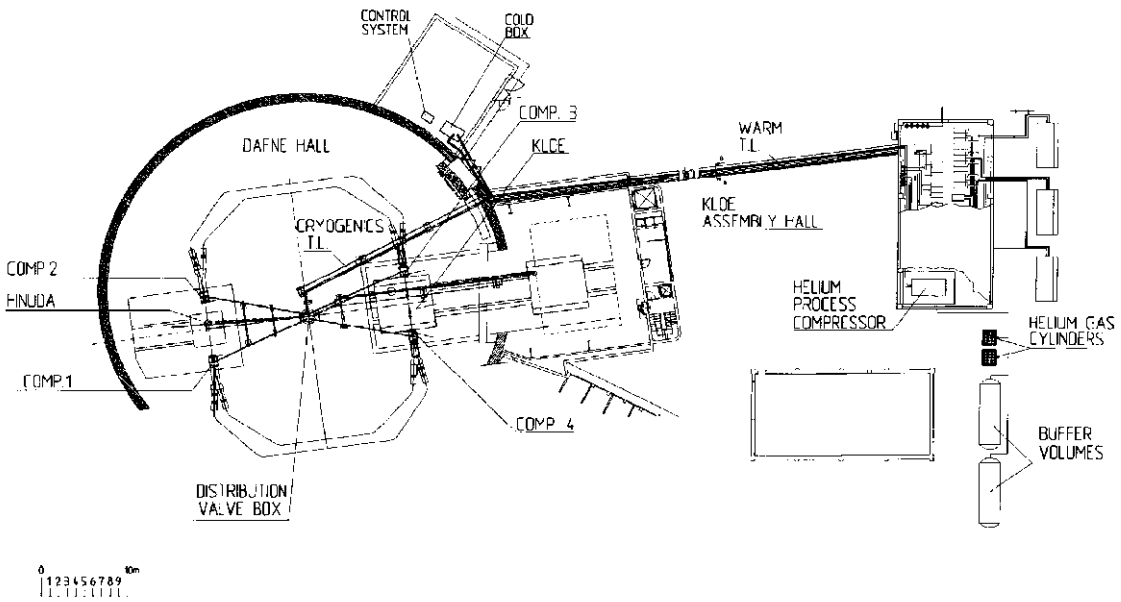

Figure 1: The DAΦNE Cryogenic System [1]

6) Distribution Valve Box, a cryogenic distribution system placed at the center of the DAΦNE hall, in the middle of the cryogenic transfer lines path. It provides the distribution of the different gas streams coming from the Cold Box to KLOE and FINUDA, but it is also designed and realized to distribute the Helium to four OXFORD INSTRUMENTS superconducting solenoid compensator magnets, (which compensate the magnetic field integral of the KLOE and FINUDA magnets, see Fig. 1).
7) Control System, a SIMATIC S7-400 PLC, connected to a remote personal computer with graphic interface. It manages almost all the valves of the system and gives information about the thermodynamic quantities related with the plant (pressures, temperatures etc.).

3 PROCESS DESCRIPTION

The cool-down process of the Cold Box is completely automatic. The control system is able to manage the plant in order to cool the Cold Box from room temperature to 4.5 K in about 3 hours.

The Cold Box has a standard Claude-Cycle design, with 2 turbines in series, 8 heat exchangers and one Joule-Thomson valve.

The most important modification with respect to the standard TCF 50 layout is the design of the cold side. Before the Joule-Thomson valve the gas flow is splitted in two parts, one passing in the Joule-Thomson valve and liquefying in a vessel, the other in a heat exchanger coil inside the vessel. This is needed to have gas at 3 bar and 4.5 K. Downstream the Cold Box the gas goes through the cryogenic transfer lines and reaches each magnet. Here there is, just before the cryostat vessel, a Joule-Thomson valve that allows the gas to liquefy.

Helium gas at intermediate temperature (≈50 K) for thermal shields cooling is supplied by the first turbine output.

So far, only the two big magnets (KLOE and FINUDA) have been cooled and energized.

KLOE is installed on the storage ring and is running since March 1999.

FINUDA has not yet rolled into the DAΦNE interaction region but it is now in its pit in the DAΦNE hall and connected to the cryogenic plant; the last cool-down took place in April 2002.

Only the two compensator magnets of KLOE have been installed. There are some problems in cooling these two magnets by means of the cryogenic plant, namely it is not possible to liquefy inside the magnet cryostat. The reason is not yet completely understood, but two possible causes are considered: first, the temperature of the gas at the end of the transfer line may be too high (due to the heat leaks in the path) for the production of liquid; second, the hole of the magnet Joule-Thomson valve may be too narrow to get the necessary flow.

Both these causes are taken in account, and some modifications are scheduled to overcome this problem (see later). At present the KLOE compensators are filled from standard liquid Helium dewars.

4 PERFORMANCE ANALYSIS

In 1997 the last installation tests of the plant have been performed and the KLOE magnet was cooled for the first time. At that time the magnet was located in a building adjacent to the DAΦNE hall. When, in 1998, the magnet was rolled inside the accelerator hall, the transfer line was modified consequently. In March 1999 the magnet was cooled and energized, and in September the experiment started the operation.

The analysis covers the period from January 2000 to May 2002. 1998/99 documentation is not accurate enough about the cryogenic faults, therefore it has not been taken into account.

From September ‘99 to spring 2002 the behaviour of the cryogenic plant is dependent on the overall efficiency of the KLOE magnet system, since the FINUDA magnet was energized only for few hours. A statistics about the faults related to the cryogenic plant is shown In Tab. 1.

False Quenches in the table are overvoltage signals in the quench detector device, that are not related with a real magnet quench but come from failures of the detector. In fact, so far, the magnet has never had a real quench. Voltage Dips are referred to the compressor mains. The Auxiliary Plants are the compressed air system (used for the valve actuators) and the water cooling plant (for the compressor and the turbines).

Most of the events, like auxiliary plant faults, KLOE PSU faults, voltage dips and false quenches, are not real cryogenics faults. However, these events are still taken into account since they originate troubles in the cryogenic plant. An important part of the downtime is due to the cryogenics restart operations following these faults.

Table 1. January 2000 – May 2002 cryogenic related faults statistics.

	Cryogenic Faults	Control System Faults	False Quenches	Voltage Dips	Auxiliary Plants Faults	Kloe PSU Faults	Not Ascribed Faults
Fault Events	5	10	2	9	8	4	5
Total Downtime (+ delivery time) [h]	40.0	42	48.5	79.0	91.5	38.5	20.5
Mean Downtime [h]	8.0	4.2	24.3	8.8	11.4	9.6	4.1

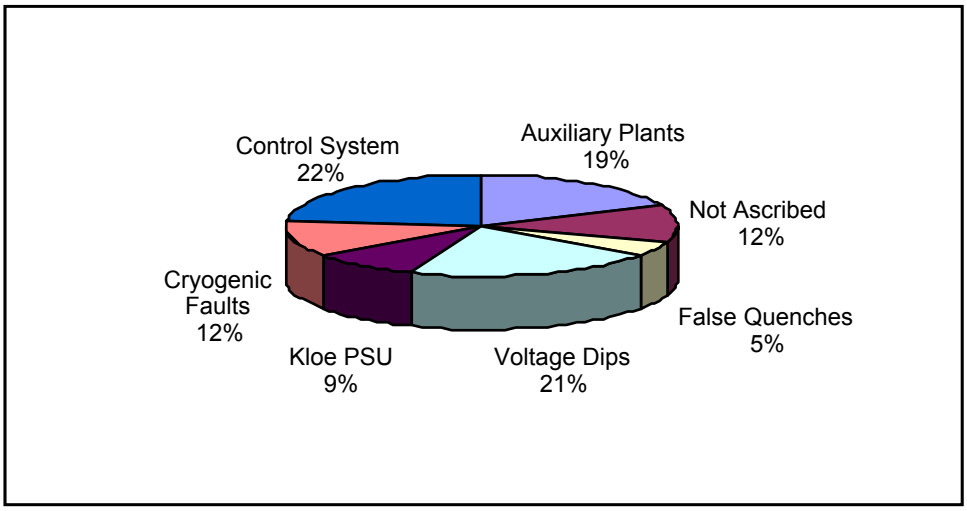

Figure 2: Relative weights of the number of events.

Real cryogenic faults are those listed in the first two columns of Tab. 1. The five Cryogenic Faults have been: a problem in a cryogenic valve, a Helium overtemperature in the KLOE inlet (two times), a problem with the compressor fan and a turbine overspeed. The Control System Faults were communication failures between the hardware electronics of the system and the PC.

Apart from the valve malfunctioning, the cryogenic faults are related to the managing of the plant in some particular conditions: a turbine overspeed can occur, for instance, when starting to cool down FINUDA while KLOE is kept cold. In this situation the request of Helium for the thermal shields suddenly increases, lowering the pressure at the output of the first turbine, increasing therefore the turbine speed.

The relative weights of the number of events are shown in fig. 2, which points out the contributions of the control system faults, the auxiliary plants faults and the voltage dips. However, if one considers the average downtime per fault, also the contribution of the false quenches is significant. To this purpose we are waiting for new quench detector boards from OXFORD Instr.

5 CRYOGENICS UPGRADES

The next shut down of the DAΦNE accelerator is scheduled in fall 2002. Several operations and upgrades are foreseen:

- Standard maintenance of the compressor and the Cold Box with cleaning of the KLOE and FINUDA magnet cryostats (including transfer lines) with pure Helium.
- Roll-in of the FINUDA magnet. Consequently, the FINUDA cryogenic transfer lines must be modified. Disconnection of the existing line and reconnection to the magnet cryostat will be performed.
- Installation of the two compensator magnets, one on each side of FINUDA experiment. These magnets were modified by OXFORD Inst. in December 2001. The 1 mm diameter Joule-Thomson valves have been replaced by 6 mm diameter new ones.
- Installation of new cryogenic transfer lines from the Valve Box to the compensator magnets. They are flexible transfer lines built by NEXANS (Germany), with an intermediate thermal shield. A small part of the cold Helium flows in the inner tube is forced to return in the thermal shield, then heated at room temperature and sent back to the compressor. The specification asks for a Helium temperature in the shields always below 25 K. In such a way the thermal power dissipated in the inner tube never exceeds 0.02 W/m.

6 CONCLUSIONS

In the period January 2000 – May 2002 the DAΦNE accelerator complex has been running for 565 days. The cryogenic plant had 15 real faults (cryogenics + control system) which caused less then 4 days of overall downtime. Other 28 faults, which stopped the cryoplant but were originated by other equipment, determined about 11 days of machine downtime.

At the moment KLOE and FINUDA are cooled by the cryogenic plant while the two KLOE compensators are cooled with helium from dewars. After the next machine shut down FINUDA and all the compensator magnets will be on the beam, and all six magnets will be cooled by the cryoplant.

7 REFERENCES

[1] M. Modena, “The DAΦNE Cryogenic System”, Rep. LNF-97/046 (IR), December 1997.

DAΦNE POWER SUPPLY SYSTEM: 5 YEARS OF EXPERIENCE AND STATISTICS

M. Incurvati, R. Ricci, C. Sanelli, LNF-INFN, Frascati, Italy

Abstract

The Power Supply (PS) System of the DAΦNE Accelerator Complex consists of about 500 PS ranging from 10 A to 3000 A and from 250 VA to 1.5 MVA. All these PS are running almost continuously since 1997. This paper, after a brief description of the entire system, reports a lot of statistics concerning about 5 years of operation, describing the main problems the different kinds of PS have been affected by, their causes and remedies. The time distribution of faults and their grouping by fault type, PS producer, etc., are reported in the form of plots and graphs.

1 INTRODUCTION

DAΦNE is an Accelerator Complex [1] consisting of:

- e^+- e^- Linac
- ≈ 180 m of Transfer Lines (T.L.)
- e^+- e^- Accumulator/Damping Ring (A.D.)
- two Storage Rings (S.R.)

The PS in the DAΦNE Accelerators are used to supply different kinds of magnets working at room temperature. The global set-up, comprehensive of T.L., A.D. and S.R., of PS is listed in Table 1.

According to the design specifications the main characteristics are:

- Three phase, 50 Hz mains voltage (V) 380±10%
- (SR Bending Dipoles) (kV) 20
- Room Temperature (°C) 0÷40
- Current Setting & Contr.Rng.(-100%) 0÷100 % f.s.
- Normal Operating Range (100%) 70÷100 % f.s.
- Current Setting Resolution $5÷20*10^{-5}$
- Current Readout Resolution $5÷20*10^{-5}$
- Residual Current Ripple $10÷20*10^{-5}$

Different typologies of PS have been adopted according to the PS output current and power rates and to the specific experience of the builder as listed below.

- SCR's Graetz Bridge Converter with Active Filtering [HAZEMEYER, OCEM]
- SCR's Graetz Bridge Converter with Transistor Output Bank [DANFYSIK, EUTRON]
- Diode's Graetz Bridge Converter with Transistor Output Bank [DANFYSIK]
- Series Double Resonant Switching Converter [OCEM]
- Zero Voltage Switching Converter [DANFYSIK]
- Hard Switching Converter [INVERPOWER]
- Bipolar Linear Converter [DANFYSIK, HAZEMEYER, INVERPOWER, FUG]
- Bipolar Switching Converter with 4 quadrant output chopper [INVERPOWER]

The analysis of faults and events covers 5 years of PS operation.

Table 1: PS characteristics

PS	N.	I_{max}(A)	V_{max}(V)
Bending Dipoles	24	100÷750	25÷1250
Dipole Back Legs	16	±10	±20
Pulsed Dipoles	3	650	1300
Wiggler Central Poles	2	750	1250
Wiggler End Poles	8	750	120
Injection Septa	8	2300	8÷50
H/V Steering	102	±10 ÷ ±215	±10 ÷ ±25
"C" Steerings	16	±215	±25
"Lambertson" Steer.	16	±215	±6
Rectang. & Square Steer.	64	±10	±20
Splitter magnets	8	750	80
Quadrupoles	143	100÷585	25÷80
Sextupoles	34	336	25÷30
Skew Quad.Currectors	16	280	40
Solenoidal magnets	4	120	10
Octupoles	6	120	20
Solenoids for experiment	2	3000	6÷10

Data have been collected in a DataBase from Control System Log-Files and Operators' Log-Books where date and type of events have been recorded since 1997. The analysis has been limited to the equipment (4 builders) installed since the beginning of the commissioning. Data are not related to builder names for privacy. MATLAB software has been used for statistics.

2 STRUCTURE OF DATABASE

The DataBase consists of 535 events (Section 3) concerning PS operation. Daily events have been collected on a suitable Time Base (TB, 14 days), to give a statistical meaning to the data. With such a grouping, 119 TB have been obtained. They are depicted in Fig.1 in steps of 30 days. A smooth curve, averaging the values over four TB (2 months), has been added. The histogram clearly points out the high first-life death rate during the operation initial period. In Nov-'98, the KLOE detector was rolled in the IP1 interaction region of the S.R. After four months of machine shut-down, the graph shows a high increase of faults and the same holds for the short (1 week) time periods of shut-down for maintenance. Maintenance, necessary for long term good operation, seems in contrast with the tendency of PS to work their best with a continuous operating cycle.

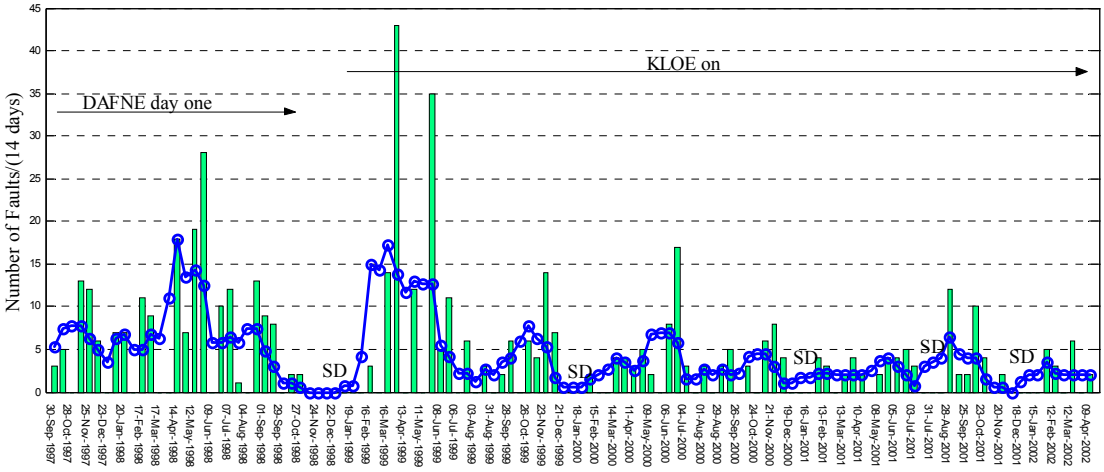

Fig.1: Faults Time Distribution

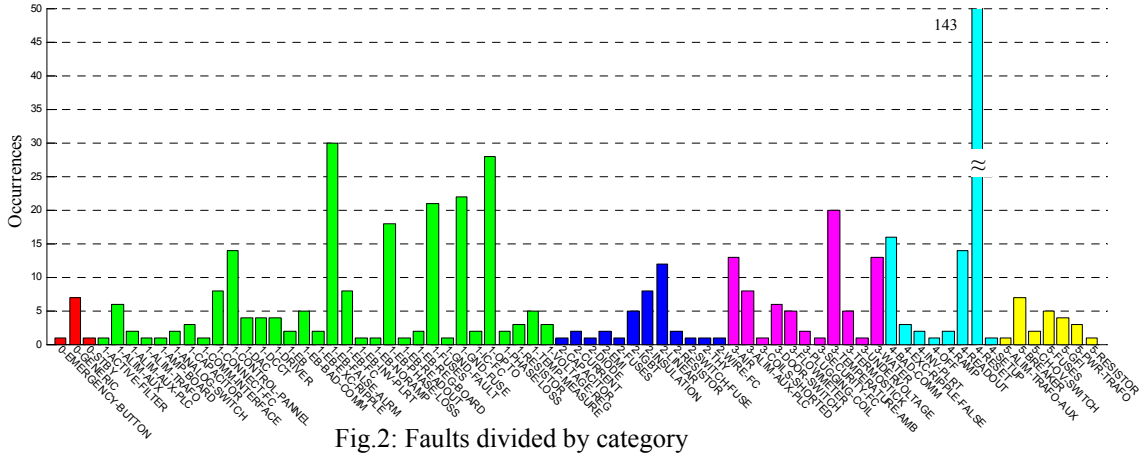

Fig.2: Faults divided by category

The average value of faults is:

$$F_{AV} = 4.47 \, faults / TB \qquad (1)$$

In the last two years F_{AV} was about 2.5 and rarely exceeded 5.

3 FAULTS CATEGORIES

To point out the critical elements of the system, faults have been divided in categories [3] as follows:

0) Generic: No significant faults.
1) Electronic: Faults concerning logic electronic elements (DAC, Optocouplers, etc.)
2) Power Electronic: Faults concerning power electronic components (IGBT, power Fuses, etc.)
3) External: Faults caused by external events (Cooling Water, Ambient Temperature, etc.)
4) Control System: Faults caused by bad interaction with network elements (Readout, Reset, etc.)
5) Electric: Faults concerning typically AC elements (Breakers, AC-Fuses, etc.)

As shown in Fig.2, faults (1), are particularly significant, even if concentrated in the first years of operation. Main troubles concerned optocouplers used in communication interfaces, electronic boards utilised for phase-loss detection, and fuses whose current rate was too stringent. Power electronic elements appear to be quite reliable. Linear components, the ones most thermally stressed, showed a higher fault rate. Also ventilation (Fans) and water cooling (water leakage) played an important role as causes of faults [2]. High external room temperature have caused the shutting down of the PS for self protection. Today, almost all PS rooms are air-conditioned and temperature is not a source of fault anymore. About Control System Interaction, troubles have been found for some PS that go to zero current without any reason (4_RESET). This is not serious problem because of a fast reset procedure. A reliability graph for any PS builder is shown in Fig.3. Three bars are presented: the first shows the total number of events occurred to each PS builder; the second relates to faults with no external events; the third shows a reliability index calculated as number of faults divided by total number of PS of the same builder.

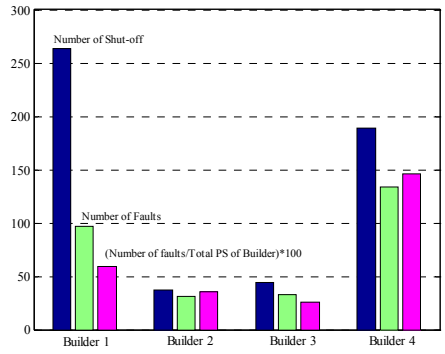

Fig.3: Builders Faults

4 STATISTICS

Some statistics calculations have been done to determine the behaviour of the PS system and foresee its behaviour. To weight the contribution of external causes, the number of Total Faults has been plotted versus the PS Faults excluding external causes for each TB (Fig.4).

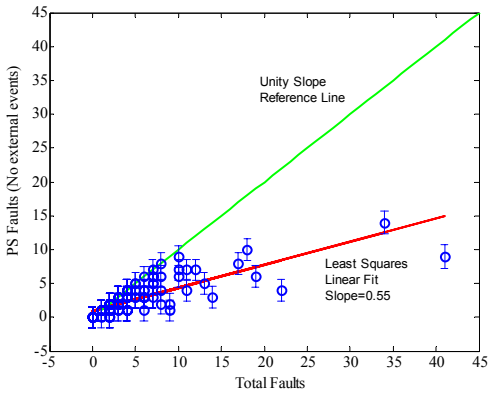

Fig.4: PS Faults (no ext.) vs. Total Faults

The unity slope line represents the equality between Total Faults and PS Faults. The dotted line is the least-squares interpolation of the scattered plot. The slope of this line can be taken as an incidence reference number of external faults. The percentile incidence of external faults can be evaluated as:

$$Ex_{\%} = \frac{1-0.55}{1} \cdot 100 = 45\% \qquad (2)$$

To evaluate the statistical behaviour of the system, the number of faults in TB has been taken as chance variable (c.v.). Occurrences of c.v. have been summed and divided by total number (119) of measurements, obtaining the probability. Thus Cumulative Probability and Probability Density plots have been derived and are shown in Fig.5. The behaviour of the system seems to be well described by Poisson distribution (dotted line). X^2 (Chi-square) goodness-of-fit test has been executed yielding Eq.(3), that, from probability tables, assures 5% statistical goodness-of-fit.

$$\chi^2 = \frac{1}{d} \cdot \sum_{k=1}^{n} \frac{(measure_k - n \cdot p_{fit,k})^2}{n \cdot p_{fit,k}} = 1.2 \qquad (3)$$

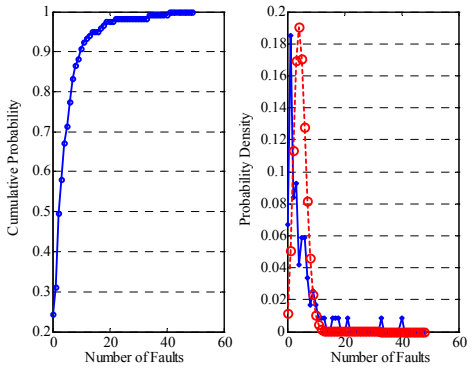

Fig.5: Cumulative and Density of Probability plots

Also an 8 months analysis of PS sensitivity to mains Voltage Dips has been done. Fig.6 shows the number of PS faults for each of the 19 recorded events. Tunings have been done on most sensitive PS to reduce the effects of Voltage Dips.

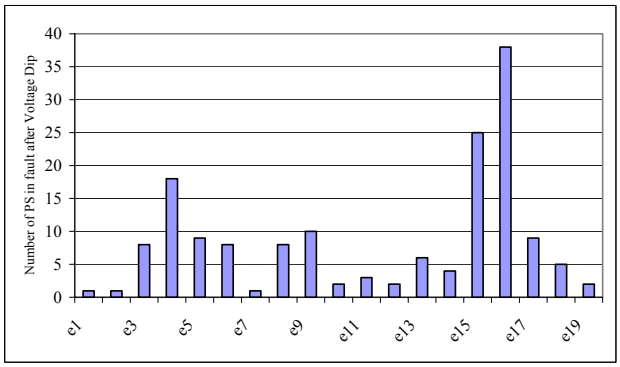

Fig.6: Voltage Dips sensitivity

5 CONCLUSIONS

PS system of DAΦNE Accelerators has been analysed showing at present a high reliability after few years of running. All PS used at LNF have fully met specifications after an initial period of tuning. The analysis points out some critical points that are currently being optimised and will be useful for future PS specifications.

6 ACKNOWELDGEMENTS

Authors whish to thank all the DAΦNE team with special attention the technicians B.Bolli, S.Ceravolo, F.Iungo, F.Sardone, for their kindness in helping to build up the database and their skill in operating the PS system.

7 REFERENCES

[1] R. Ricci, C. Sanelli, A. Stecchi: “DAΦNE Magnet Power Supply System”, EPAC’98.

[2] L. Pellegrino: “The DAΦNE Water Cooling System”, EPAC’98.

[3] Dan Wolff, Howie Pfeffer: “Experience in Mantaining and Operating Power Supplies Used in Accelerators”, EPAC’96

DAΦNE BROADBAND IMPEDANCE

A. Ghigo, D. Alesini, C. Biscari, A. Drago, A. Gallo, F. Marcellini, C. Milardi, M. Serio, M. Zobov,
LNF-INFN, Frascati, Italy

Abstract

Beam dynamics is one of the most challeging issues of DAΦNE, due to the high single bunch current involved. The single bunch dynamics is dominated by the short range wakefields, that are usually expressed in terms of machine broad band impedance. Measurements of bunch lengthening and betatron tunes as functions of bunch currents have been performed on both rings to evaluate the longitudinal and transverse broadband impedances. Results are compared with calculations and impedance differences between the two rings are discussed.

1 INTRODUCTION

The Φ–factory DAΦNE is a e^+e^- collider at the energy of the Φ resonance (1020 MeV in the center of mass) designed and built in Frascati National Laboratories of INFN [1]. It is aimed at producing a very high luminosity in the 10^{32} $cm^{-2}s^{-1}$ range. Longitudinal and transverse beam dynamics in DAΦNE are crucial, since the strategy chosen to get the required high luminosity calls for high values of both single and multibunch currents. At present, the design single bunch current of 44 mA has been largely exceeded in both collider rings: about 200 mA have been stored in a single bunch without observing harmful instabilities. In the multibunch regime more than 2 A of average current have been stored in the electron storage ring and about 1.3 A in the positron one. In this paper we discuss the single bunch dynamics, while multibunch dynamics aspects are considered elsewhere [2]. In particular, we study the machine broadband coupling impedance describing parasitic interaction of a bunch with the surrounding vacuum chamber. In the longitudinal plane this can be done by measuring and analyzing bunch lengthening and microwave instability. These issues are very important for the low energy collider DAΦNE since the lifetime, dominated by the Touschek effect, grows proportionally to the bunch length. On the other hand, an excessive bunch lengthening may lead to luminosity performance limitation due to the "hour-glass" effect. In turn, in the microwave regime, unstable internal bunch oscillation modes can worsen injection and create new destroying resonances in beam-beam collisions. In the transverse plane, short range wake fields cause betatron tune shift and, in the worst case, can result in the turbulent mode coupling instability, putting severe restriction on the bunch current. Section 2 of this paper describes the experimental set up for the bunch length measurements, while the experimental results, longitudinal broad band impedance estimates and comparison with analytical calculations and numerical simulations are given in Section 3.

In Section 4 we summarise the results of the transverse broad band impedance measurements.

2 MEASUREMENT SETUP

DAΦNE synchrotron light in the visible range of the radiation, emitted by the electrons and the positrons in dipole magnets symmetrically placed in the two rings, is transported to an external laboratory through two 25 m long optical lines. In this configuration, with the identical length of the two optical lines, simultaneous measurements on the two beams (also during interaction) are feasible without any change of the experimental set-up.

In each line a water-cooled Al mirror extracts the radiation from the antechamber of the vacuum pipe through a fused silica vacuum window. The light passes a 2 mm aperture slit which limits the source path to 3 mm in order to have temporal resolution better than 10 ps. Two large aperture achromatic lenses and a series of glass mirrors with surface metallization transport the light up to the optical bench outside the DAΦNE hall in which the measurement systems are installed.

The bunch length is measured with a Streak Camera Hamamatsu C5680 with 1.5 ps resolution. The camera operates in synchroscan mode, in which the fast sweep is triggered by an internal RF signal locked to the machine RF. In order to use a Hamamatsu commercially available circuit we trigger with the fourth sub-harmonic of the master oscillator (368/4 = 92 MHz). The single bunch longitudinal distribution is recorded with variable integration time (1-100ms) depending on the bunch current. The incoming trigger jitter, which can affect the measurements overestimating the bunch length, has been measured: its rms value is less than 4.5 ps. During the measurements the stability of the longitudinal position of the bunch has been verified by monitoring an electromagnetic pickup signal with a spectrum analyser. The streak camera signals are stored in a PC and analysed initial-time with a Hamamatsu software to give the full width at half maximum value of the pulse length. More complete analysis is performed extracting the pulse profiles data and fitting them off-line.

3 BUNCH LENGTH AND IMPEDANCE MEASUREMENTS

We have performed bunch length measurements at different RF voltages V_{RF} and varying the momentum compaction α_c. Figures 1 and 2 shows the bunch length σ_z for the positron and electron rings, respectively. The RF voltages and momentum compactions for each set of measurements are indicated in the corresponding plot legends. In these plots we note that above certain current

thresholds bunch lengthening no longer depends on the momentum compaction and can be described by simple scaling laws:

$$\sigma_z[cm] = 4.36 \times \left(\frac{I[mA]}{V[kV]}\right)^{1/3} ; for \quad positron \quad ring$$

$$\sigma_z[cm] = 5.50 \times \left(\frac{I[mA]}{V[kV]}\right)^{1/3} ; for \quad electron \quad ring$$

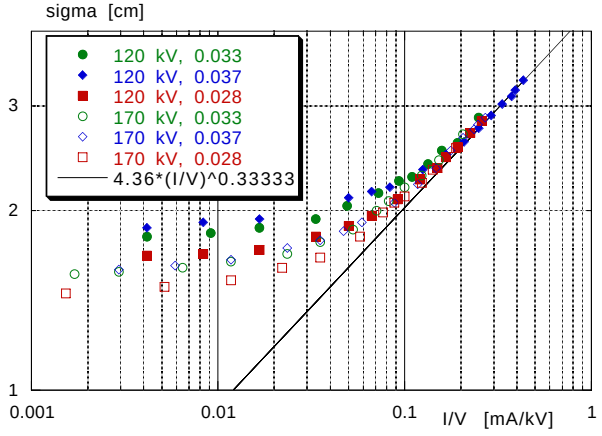

Figure 1: Bunch lengthening in e^+ ring.

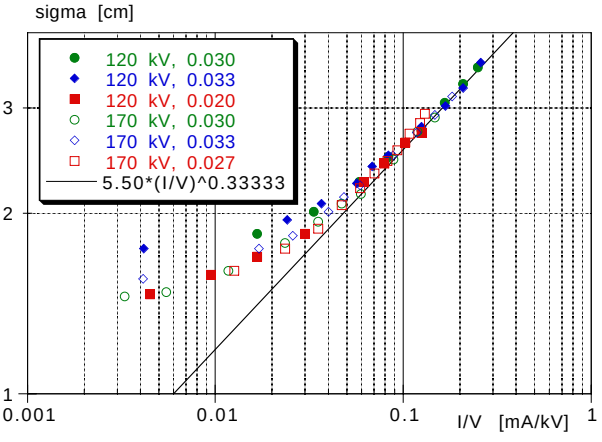

Figure 2: Bunch lengthening in e^- ring.

As it has been shown [3], for a given storage ring, the bunch length satisfies the following scaling property above the microwave instability threshold:

$$\sigma_z = f(\xi)$$

where the scaling parameter ξ does not depend on momentum compaction:

$$\xi = \frac{\alpha_c I}{\nu_s^2 E} = \frac{2\pi I}{heV_{RF}\cos\varphi_s}$$

Here E is the storage ring energy; h the harmonic number; ν_s the coherent synchrotron tune; ϕ_s the synchronous frequency and e the electron charge.

The fact that in our case the bunch length scales as

$$\sigma_z \propto \xi^{1/3}$$

shows that the effective longitudinal coupling impedance is practically purely inductive. This is not a surprise since the bunch in DAΦNE is relatively long at the nominal current and the effective impedance "seen" by the bunch is dominated by the low frequency inductive impedance of the vacuum chamber. From the above scaling laws the impedance is evaluated to be 0.53 Ω for the positron ring and 1.1 Ω for the electron one. The significant difference between the impedances of the two rings (by a factor 2) can be explained, in our opinion, by the presence of 40 ion clearing electrodes in the electron ring. Figure 3 shows the measured bunch distribution profiles at low current and at the nominal current for the electron ring. As it can be observed, the bunch gets much broader due to interaction with the inductive impedance and slightly asymmetric due to the real part of the impedance. The shift of the bunch center corresponds to the synchronous phase shift due to small, but not negligible parasitic energy losses.

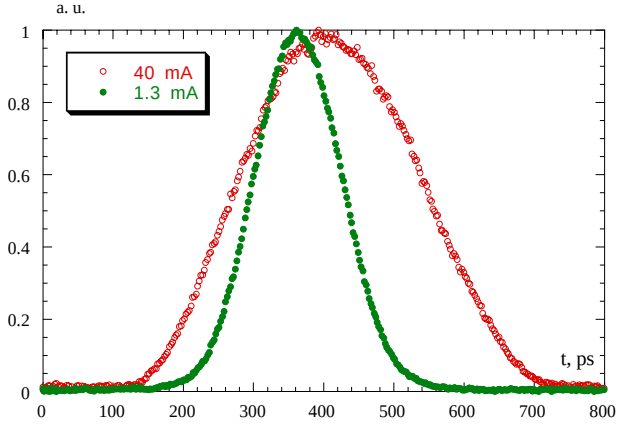

Figure 3: Bunch density profiles at low and high current.

Yet another observation is that the bunch enters the turbulent regime (see points reaching the straight lines in Figs. 1, 2) at higher currents for lower RF voltages and higher momentum compactions. This is in agreement with Boussard's criterion on the higher instability thresholds for lower peak currents. The microwave instability does not seem to be harmful to beam dynamics. In the worst case we observe unstable quadrupole oscillations on the spectrum analyzer at high currents per bunch that can be damped by lowering the RF voltage.

It is worth mentioning that the measured impedance is in a good agreement with analytical calculations and numerical simulations carried out much prior to DAΦNE commissioning. At the very early stage of the vacuum chamber design the applied broadband impedance model [4] predicted for DAΦNE had the following frequency dependent impedance:

$$\frac{Z}{n} = \left\{ \begin{array}{l} -i0.26 + \dfrac{24.8}{n} + \dfrac{\left(1 - i\,\mathrm{sgn}(n)\right)2.89\sqrt{|n|}}{n} + \\ + \dfrac{\left(1 + i\,\mathrm{sgn}(n)\right)274.42}{n\sqrt{|n|}} \end{array} \right\} \Omega$$

The estimate of the impedance at the bunch spectrum roll-off frequency for the nominal bunch length of 3 cm gives |Z/n| = 0.41 Ω, close to the measured positron ring impedance. Later, the overall short range wake function was calculated numerically by adding up contributions of almost all the vacuum chamber discontinuities [5] assuming a 2.5 mm gaussian bunch. The resulting wake function and the broadband impedance (Fourier transform of the above wake field) are shown in Fig. 4 and Fig. 5, respectively. It can be pointed out that the |Z/n| value is about 0.6 Ω for almost all the 2.5 mm bunch frequency spectrum. The results of bunch lengthening process simulations based on the given wake function have already shown a good agreement with previous measurement results in the positron ring performed by detecting and elaborating the beam signal induced in a broadband button electrode [6].

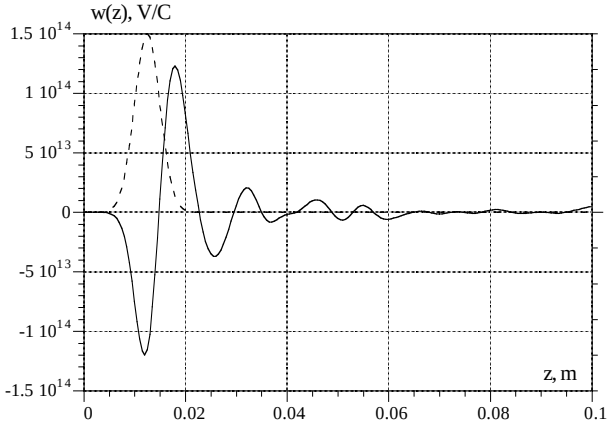

Figure 4: Wake field of a 2.5 mm Gaussian bunch.

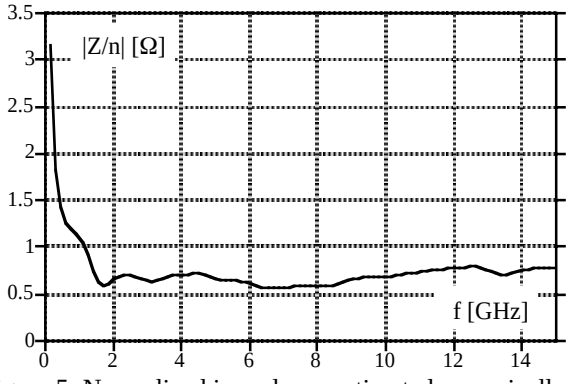

Figure 5: Normalized impedance estimated numerically.

4 TRANSVERSE IMPEDANCE

We estimated the transverse effective impedance Z^{eff} by measuring the dependence of the coherent betaron frequency of the dipole mode (m = 0) on the bunch current. The imaginary part of the impedance is proportional to the measured current dependent betatron frequency shift Δf:

$$\mathrm{Im}\left\{Z_{\perp}^{eff}\right\} = \frac{\Delta f \sigma_z}{I}\,\frac{32\pi^2 f_0 Q(E/e)}{c^2}$$

where Q is the betatron tune (either vertical or horizontal); f_0 the revolution frequency; and c the speed of light.

Figure 6 shows the betatron frequency shifts as a function of the bunch current measured in the electron ring (empty circles) and in the positron one (full circles). The two upper curves correspond to the frequency shift in the horizontal plane while the lower ones show the results of the vertical frequency shift measurements. Due to the shape of the vacuum chamber, the vertical tune shift is higher than the horizontal one for both rings. The vertical frequency shift curves are similar for the two rings, but the transverse impedances are different since the bunch is longer in the electron ring. For the nominal bunch current of 40 mA, the effective impedances are evaluated to be equal to 165 kΩ/m and 130 kΩ/m for the electron and positron rings, respectively. It is noteworthy that the vertical impedance of the electron ring is by a factor of 4 higher than the horizontal one, while in the case of the positron it is only 2. This difference is still to be understood.

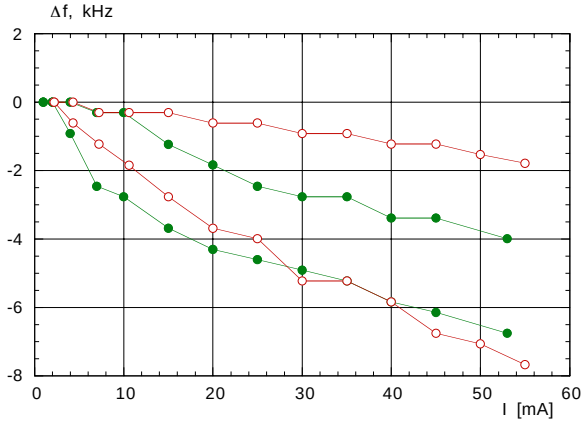

Figure 6: Measured betatron tune shifts vs. bunch current.

We also can conclude that we are safely far from the transverse turbulent microwave instability threshold, since the measured frequency shifts at the nominal bunch current are much smaller than the synchrotron frequency, which varies in the range 25÷40 kHz depending on applied RF voltages and momentum compaction.

5 REFERENCES

[1] G. Vignola, “DAΦNE, The Frascati Φ-Factory,” PAC’93, Washington, 1993.

[2] A. Drago et. al., this conference, THBGB001.

[3] A. W. Chao, J. Gareyte, “Scaling Law for Bunch Lengthening in SPEAR II”, Part.Accel. 25: 229, 1990.

[4] M. Zobov et. al., “Broad-band Model Impedance for DAΦNE Main Rings”, NIM A 337 (1994), 231 - 241.

[5] M. Zobov et. al., “Collective Effects and Impedance Study for the DAΦNE Φ – Factory”, KEK Proceedings 96-6, August 1996 (A).

[6] M. Zobov et. al., “Bunch Lengthening and Microwave Instability in the DAΦNE Positron Ring”, DAΦNE Technical Note: BM-3. Frascati, June 7, 1998.

BEAM LIFETIME STUDIES IN DAΦNE

S. Guiducci, LNF-INFN, Frascati, Italy

Abstract

The beam lifetime of the DAFNE Φ-factory is strongly dominated by the Touschek effect. An analysis of its dependence on machine parameters has been done in order to improve machine performance. Measurements taken in different conditions are here presented and compared with simulations. The agreement is quite satisfactory when taking into account the measured bunch length, the machine coupling, and the estimated dynamic aperture.

1 INTRODUCTION

Two experiments, KLOE and DEAR, are taking data on the DAΦNE Φ-factory [1]. During KLOE data taking the average DAΦNE luminosity is a large fraction (70%) of the peak one even if the beam lifetime is quite short. The lifetime of the two beams ranges between 15 and 30 min, the luminosity is mantained close to the peak value all the time by frequent beam refills (every 10-15min), while KLOE data acquisition is kept on.

A further step to increase average luminosity necessarily requires dedicated work to improve beam lifetime. In fact, as it will be described below, tuning the machine to increase peak luminosity generally has a side effect of reducing lifetime. A short beamlifetime is also related to a high machine background in the detectors. The different actions adopted to reduce the background level are described in [2].

DAΦNE beam lifetime is determined by the single Touschek scattering and by the interaction with gas molecules (scattering and bremsstrahlung). Among the two effects the Touschek is the dominant one, due to the relatively low energy and the very good vacuum.

2 BEAM LIFETIME CALCULATIONS

To calculate the beam lifetime for DAFNE the computer code LEDA [3] has been modified in order to take into account the actual shape of the vacuum chamber and the limit due to the dynamic aperture [4].

Touschek effect is an elastic scattering of two particles within a bunch. The two emerging particles suffer the same change of the relative momentum devlation ε, one gains and the other loses.

Lifetime is calculated according to the formula given by H. Bruck[5]:

$$\frac{1}{\tau} = \frac{\sqrt{\pi}\, r_o^2 c N}{\gamma^3 \sigma'_x\, \varepsilon^2 (4\pi)^{\frac{3}{2}} \sigma_l \sigma_x \sigma_y} C(u_{min}) \qquad (1)$$

where: r_0 classical electron radius, c velocity of light, γ electron energy in units of rest mass, N number of electrons per bunch, $(4\pi)^{3/2}\ \sigma_l\ \sigma_x\ \sigma_y$ bunch volume,

$$\sigma_x' = \sqrt{\varepsilon/\beta_x + \sigma_p^2 (D_x' + D_x \alpha_x/\beta_x)^2}$$

and $C(u_{min})$ is a slowly varying function of $u_{min} = (\varepsilon/(\gamma\sigma_x'))$. ε is the maximum accepted value for the relative momentum deviation. It is the minimum between RF acceptance and momentum acceptance due to transverse aperture (physical or dynamic).

At each azimuth s_i along the ring the following quantity is calculated:

$$H(s_i) = \gamma_i D_i^2 + 2\alpha_i D_i D'_i{}^2 + \beta_i D'^2_i . \qquad (2)$$

The maximum horizontal displacement in a position s_j for a particle which has got a relative momentum deviation change ε_i in s_i is:

$$x_j = \varepsilon_i \left[\sqrt{H_i}\, B_j + |D_j| \right] \qquad (3)$$

The limiting value for ε_i is obtained by equating x_j to the physical half-aperture in that position A_x^j and taking the minimum all over the ring:

$$\varepsilon_i = min_j \left\{ \frac{A_x^j}{\sqrt{H_i \beta_i} + |D_j|} \right\} \qquad (4)$$

The minimum between ε_i and ε_{RF} is used to calculate at s_i the value of $1/\tau$ which is then averaged over the ring. To take into account dynamic aperture, a value for the aperture limit at different energies is given in input, at a fixed azimuth, assuming it scales as square root of β_x along the ring.

The total beam lifetime is calculated taking into account quantum lifetime, Touschek scattering, elastic and inelastic gas scattering.

The DAFNE parameters used to calculate the beam lifetime for a typical configuration are listed in Table 1 and the different contributions to the total lifetime are shown in Table 2. This calculation is performed using the vacuum chamber aperture without including dynamic aperture limitation.

Table 1: Parameters used for lifetime calculations

E = 510 MeV	V_{RF} =120KV
ε = 0.94 mm mrad	ε_{RF} = 6.0 10^{-3}
α_c = .030	σ_l = 2.2 10^{-2} m
U_0 = 9.2 KeV	I_{bunch} = 15 mA
σ_p nat = 4.0 10^{-4}	κ = 2.0 10^{-3}

Table 2: Different contributions to DAFNE lifetime

Quantum lifetime	$1.7\ 10^{35}$ s
Gas bremsstrahlung	$1.08\ 10^{5}$ s
Gas scattering	$1.01\ 10^{5}$ s
Touschek	2567 s
Total	2447 s

A value of gas pressure of $T10^{-9}$ torr is assumed, in practice the average vacuum is well below this value. Anyway the beam gas contribution is much smaller than the Touschek, due to the low energy of the ring and to the very small value of the vertical emittance. In fact τ is proportional to γ^3 and σ_y (see (1)).

2.1 Lifetime limitations

In practice the measured lifetime is smaller than the calculated one and therefore the factors that could give a lifetime reduction have been studied. The main possible limitations are: closed orbit, coupling configuration and dynamic aperture.

Closed orbit is not included in the calculations and could reduce the effective aperture. After correction the closed orbit is displaced by means of orbit bumps along the ring to check that it is not affecting beam lifetime. This is specially useful in the interaction regions where, due to crossing angle at the interaction point, the two beams travel off axis.

Coupling is measured from the ratio R ($R = \sigma_y / \sigma_x$) at synchrotron light monitor (SLM). The resolution of the SLM could affect this measurement and the difference between the coupling measured at the SLM and its value around the ring might explain a discrepancy in the measured and calculated lifetime. Coupling is corrected down to very small values by using antisolenoids to compensate the strong effect of KLOE solenoid and then by adjusting eight skew quadrupoles in each ring.

A dynamic aperture smaller than the vacuum chamber could explain the short lifetime. In fact lifetime is very sensitive to sextupole settings and betatron tunes. DAΦNE is a small machine with two low β interaction regions and therefore has strong chromaticity correcting sextupoles.

Beam measurements have shown the presence of a strong nonlinear term in the field of the wigglers [6]. This nonlinear term gives a large tune shift on amplitude and a reduction of the dynamic aperture. Octupole magnets have been recently installed to compensate this effect, preliminary results are presented at this conference [7].

3 MEASUREMENTS

In order to understand the beam lifetime behaviour different kinds of measurements have been performed. Only measurements performed with positrons are shown because with electrons the ion trapping effect makes the interpretation of the data less clear. For electrons beam lifetime is longer due to larger coupling and longer bunches.

3.1 τ versus Beam Current

It is important to know the dependence of τ on the current in order to correctly normalize measurements done at different currents. As shown in (1) Touschek lifetime is inversely proportional to current. For the operating currents the bunch length is in the anomalous lenghtening regime [8] and its length is proportional to $I^{1/3}$. As a consequence lifetime is proportional to $I^{-2/3}$.

Beam lifetime τ as a function of current, in the DEAR configuration, at a coupling $\kappa = 3.4\ 10^{-3}$ is shown in Fig. 1: triangles are measured points and the line is a fit with $I^{-2/3}$.

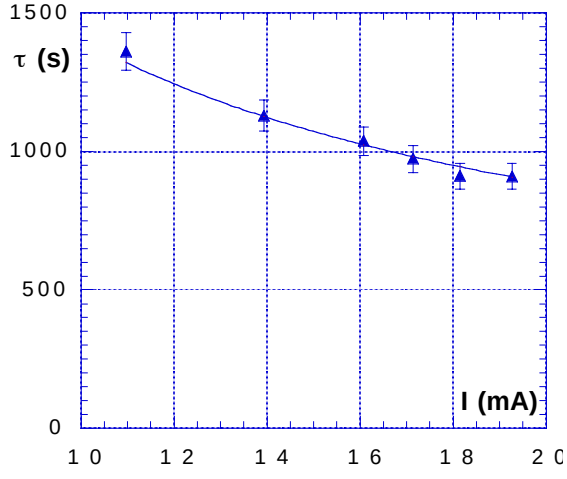

Figure 1: Measued lifetime versus current fitted with $\tau \propto I^{-2/3}$.

3.2 Lifetime versus skew quadrupole current

From (1) a linear behaviour of τ versus the vertical beam size σ_y is expected. We vary machine coupling by changing the current of a skew quad and measure the ratio R at the SLM. We use the ratio R instead of σ_y because it is less sensitive to the intensity of the beam image (the horizontal beam size is constant during the measurement because the coupling is very small).

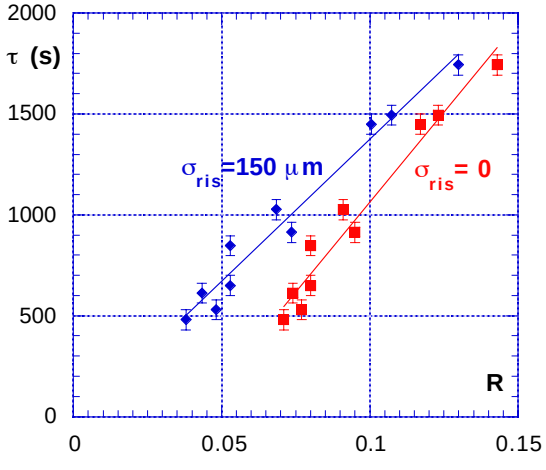

Figure 2: τ vs. R with and without SLM resolution.

The squares in Fig. 2 show the beam lifetime versus R for a single bunch in the KLOE collision configuration at currents of 10 mA. The points are fitted with a straigth line. Due to the effect of the resolution of the SLM the line does not cross zero. Data are corrected by subtracting quadratically the SLM resolution in order to have a line crossing through zero. The horizontal beam size is σ_x = 2.4 mm, and therefore the minimum measured value of R = .075 corresponds to a resolution σ_{ris} = 150 μm and a vertical size σ_y = 108 μm.

3.3 τ versus RF Voltage

The RF energy acceptance increases with the square root of the RF voltage. Touschek lifetime increases with the square of the energy acceptance (neglecting the function $C(u_{min})$ nearly constant in our case) and therefore it should increase linearly with the voltage if there were no other limitations due to physical and dynamical aperture. A dynamic aperture limitation at 7 σ_x has been estimated by inserting a scraper to intercept the beam and an energy limitation of .5% has been observed when changing the energy by means of RF frequency. The measured (April 01) behaviour of lifetime as a function of RF voltage is shown in Fig. 3 (dots) and compared with calculations. The solid line is the lifetime calculated taking into account the vacuum chamber aperture (larger than 10 σ_x all over the ring), and the measured bunch length. A coupling value of $\kappa = 2.3\ 10^{-3}$ has been used instead of $\kappa = 4.5\ 10^{-3}$, given by the SLM, due to the fact that the beam size is smaller than the SLM resolution. Such a low coupling value is measured by the luminosity scans made (at low current) by varying the vertical position of one of the beams at the crossing point. From this scan a value of $\Sigma = \sqrt{\sigma_{y+}^2 + \sigma_{y-}^2} = 11\mu m$ has been obtained. The dashed line, which fits the data, assumes a dynamic aperture limitation at 7 σ_x and an energy limitation of .5%.

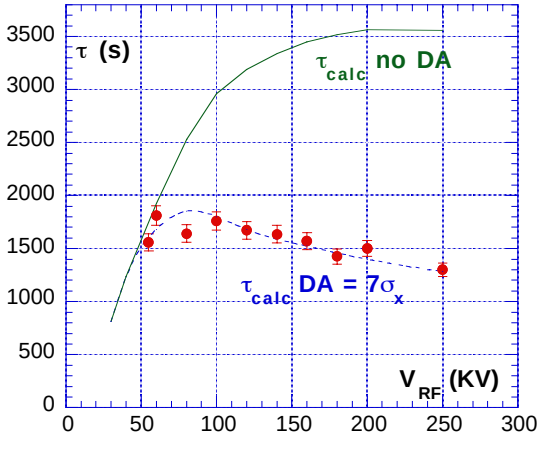

Figure3: τ vs. V_{RF}, I = 10 mA, $\kappa = 2.3\ 10^{-3}$.

This plot shows a strong reduction of lifetime due to dynamic aperture limitations.

On the KLOE optics machine coupling has been continously reduced in order to increase the luminosity. The vertical β_y at the IP has been reduced from .06 m to .03m. This change has improved the luminosity at the expense of increased chromaticity and sextupole strengths which could reduce the dynamic aperture. Luminosity has increased from 2.0 $10^{31}cm^{-2}s^{-1}$ (Apr 01) to 5.1 $10^{31}cm^{-2}s^{-1}$.

Recent measurements (May 02) on the KLOE optics (see Fig. 4) show a smaller lifetime. The measurements have been performed for two different values of R and scaled at the same value of $\kappa = 1.8\ 10^{-3}$ taking into account SLM resolution. The Σ measured by luminosity scans is Σ = 7.9 μm and corresponds to a lower coupling $\kappa = 1.1\ 10^{-3}$.

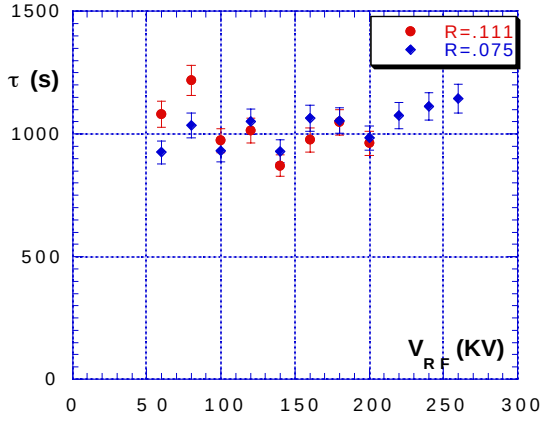

Figure 4: τ vs. V_{RF} at 10mA and $\kappa = 1.8\ 10^{-3}$ taking into account the SLM resolution.

5 CONCLUSIONS

The measured beam lifetimes are in reasonable agreement with calculations when taking into account dynamic aperture, measured bunch length and coupling. Very small coupling and strong nonlinearities give a quite short lifetime. A chance to improve the lifetime will come from the present work dedicated to study machine nonlinearity and increase the dynamic aperture.

6 REFERENCES

[1] M. Zobov et al., “Luminosity Performance of DAFNE”, This Conference.
[2] M. Boscolo et al., “Simulations and measurements of the Touschek Background at DAFNE”, This Conference.
[3] G. Vignola., “LEDA code,” private communication.
[4] S. Guiducci., “Beam Lifetime in DAFNE”, DAFNE Technical Note L-12, February 1993.
[5] H. Bruck, “Accelerateurs Circulaires de Particules”, Presse Universitaires de France, 1966.
[6] C. Milardi et al., “Effects of nonlinear terms in the wiggler magnets at DAFNE”, PAC 2001, Chicago, USA, 2001.
[7] C. Vaccarezza et al., “Preliminary Results of DAFNE Operation with Octupoles”, This Conference.

PRELIMINARY RESULTS ON DAΦNE OPERATION WITH OCTUPOLES

C. Vaccarezza, M.E. Biagini, A. Drago, C. Sanelli, F. Sgamma, M. Zobov, INFN-LNF, Frascati, Italy

Abstract

Octupole magnets have been installed in the DAΦNE e^+ e^- collider to compensate an octupole-like component measured in the wiggler magnets, so providing a knob to control unwanted non linear terms. DAΦNE operation is presently shared between two experiments : KLOE, measuring CP violation in Kaon decays, and DEAR studying exotic atoms. In the following, preliminary results on DAΦNE operation with octupoles and comparison with simulations are presented.

1 INTRODUCTION

The high order multipole terms in the magnetic field of the wiggler magnets of the DAΦNE e^+ e^- collider [1], mostly account for the measured betatron tune shift dependence on the particle oscillation amplitude and residual second order chromaticity. These non-linear magnetic fields affect the dynamic aperture, the beam lifetime (strictly connected with background and noise rates of the experiments), and the beam-beam performance. To simulate the consequences of such a multipolar effect in the machine model, an octupole term has been added to each wiggler, with an integrated strength of $K_3 l = 1000 \mathrm{m}^{-3}$ [2], in order to fit the non-linear coefficient of the chromaticity. To provide a knob for compensating the cubic non-linearities it has been decided to install octupole magnets in both rings with the same integrated maximum strength [3]. Three of them were installed in both rings in January 2002, as indicated in Fig. 1. This configuration has been chosen as the most feasible and less perturbative for the original machine layout. The main parameters of the magnets are reported in Table 1. In parallel with the routine operation for the experiments some work has been done to optimize the machine behaviour with the octupoles. In the following section the correction of the amplitude dependent tune shift effect and the second order chromaticity of the machine with the octupoles is described. A comparison between the simulation and the single beam experimental results coming from the octupole compensated lattice is discussed. In the last section results on octupole and sextupole tuning for the DEAR experiment configuration are presented.

2 FIRST RESULTS WITH SINGLE BEAM

The non-linear behaviour of the machine has been investigated in single beam mode. In particular, betatron tune measurements as a function of horizontal closed orbit bumps inside the wiggler magnets have shown that the tune dependence on the bump amplitude has a parabolic behaviour, on average comparable in the two

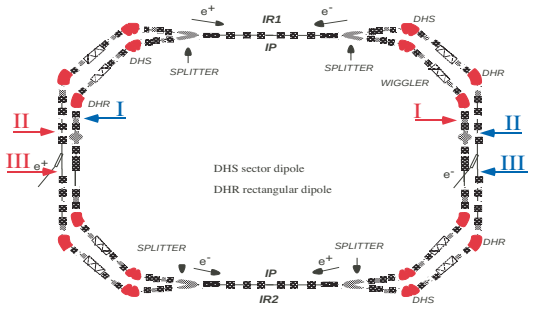

Figure 1: DAΦNE positron and electron ring layout with the octupole magnets location, (three magnets per ring, blue and red color marker respectively).

Table 1: DAΦNE octupole magnet parameters

Octupole constant	$K_3 l = 1000\ \mathrm{m}^{-3}$
Magnetic Length	$l = 0.1$ m
Bore radius	$a = 0.05$ m
Max excitation current	120 A
Current density	7 A/mm^2

rings, disappearing when the wigglers are switched off [2]. In order to study this effect, chromaticity and beam decoherence measurements have been performed on different lattices, with the wiggler magnets powered on and off [4]. The beam decoherence is measured by kicking a single bunch horizontally, using one of the injection kickers. A dynamic tracking system [5] allows to store turn-by-turn the position of the kicked bunch. The cubic non-linearity is then estimated by fitting the decoherence signal envelope. The results have proven that the wigglers are a strong source of both the second order chromaticity and the tune dependence on the oscillation amplitude. From the analysis of the wiggler magnetic measurements this cubic contribution is found to arise from the superposition of an actual fourth order term in the magnetic field and the horizontal wiggle (about 25 mm peak-to-peak) of the beam trajectory [6].

2.1 Amplitude Dependent Tune Shift

The tune shift of betatron oscillations due to octupoles can be calculated analytically:

$$\Delta Q_x = \frac{J_x}{16\pi} \int \frac{\partial^3 B}{\partial x^3} \frac{1}{(B\rho)} \beta_x^2(s) ds \approx \frac{J_x}{16\pi} \frac{K_3 l \bar{\beta}_x^2}{32\pi} \qquad (1)$$

where J_x is the horizontal action variable.

From the decoherence measurements [5] we can obtain the c_{11} coefficient, characterizing the strength of the cubic

non-linearity:

$$c_{11} = \frac{\Delta Q_x}{2J_x} = \frac{K_3 l \bar{\beta}_x^2}{32\pi} \qquad (2)$$

In order to check the octupole contributions to the lattice cubic non-linearity we have compared the measured c_{11} (estimated from the difference of the c_{11} coefficient measured with the octupoles on and off), and the c_{11} value obtained from the above analytical formula, using the beta functions provided by the linear optics model. The results are in good agreement as shown in Table 2.

2.2 *Second Order Chromaticity*

The second order chromaticity contribution of an octupolar term can be obtained from the general equation of the betatron motion when terms up to the second order in $\delta = \frac{\Delta p}{p}$ are considered. Keeping only the terms linear in the horizontal coordinate, x_β, the gradient error can be expressed as :

$$\Delta\kappa = -[(\kappa - m\eta_x)\delta - (\kappa - m\eta_x + \frac{1}{2}r{\eta_x}^2)\delta^2] \qquad (3)$$

where $m = \frac{l}{B\rho}\frac{\partial^2 B}{\partial x^2}$, $r = \frac{l}{B\rho}\frac{\partial^3 B}{\partial x^3}$, and η_x is the horizontal dispersion function.

Considering only the contribution coming from wigglers and octupoles, the resulting tune shift is given by:

$$\Delta Q_x = \frac{1}{8\pi}\oint [\beta_x r {\eta_x}^2 \delta^2]_{wigglers} + \frac{1}{8\pi}\oint [\beta_x r {\eta_x}^2 \delta^2]_{octupoles} \qquad (4)$$

A similar formula holds for the vertical plane.
The second order coefficients of a polynomial fit for the chromaticity measurements, performed with the DEAR lattice for the positron ring under different conditions, are reported in Table 3. Each octupole was powered at half of the maximum current, the sextupole magnets were always switched off. In the first column the second order coefficient is obtained by fitting the measurements, in the second one the same obtained by fitting the MAD [7] results for the computed ΔQ vs δ with the measured octupole term in the wigglers. The result of eq. 4 is given in the third column. The agreement is quite good for the horizontal plane, somewhat worse for the vertical one. By solving the system given by eq. 4 and its analogous for the vertical plane, it is possible to compensate the second order chromaticity coming from the wiggler magnets. Chromaticity measurements performed on the e^+ ring for the KLOE optics, for the two cases with and without the calculated correction, are shown in Fig. 2. The applied correction is about the 60% of the total calculated one; the second order coefficient of the fit is reduced from ≈ -760 down to ≈ -160 in the horizontal plane and from $\approx +640$ down to $\approx +130$ in the vertical one. The energy acceptance is also increased.

Table 2: Lattice cubic non-linearity, c_{11} coefficient values, calculated and measured.

Element	$K_3 l$ [m^{-3}]	c_{11}^{meas}	c_{11}^{calc}
OCTPL101	500	-30	-40
OCTPS101	500	+140	+130
OCTPL201	500	+110	+100

Table 3: The second order coefficient of the polinomial fit of the ΔQ vs δ curve, (horizontal and vertical plane), obtained from measurements, simulation and analytical estimates.

Horizontal plane

Element status	exp	Mad	anal.est.
Octupoles off	-1200	-1200	-1250
OCTPL101 on	-1100	-1480	-1390
OCTPS101 on	-1200	-1230	-1200
OCTPL201 on	-600	-460	-710

Vertical plane

Element status	exp	Mad	anal.est.
Octupoles off	680	250	590
OCTPL101 on	1340	1200	1000
OCTPS101 on	840	440	590
OCTPL201 on	520	-100	150

Tracking results, performed for the same lattice with octupoles on and off, showed a 20% horizontal enlargement of the dynamic aperture, obtained with 40% of this former correction, and a 30% vertical shrink, see Fig. 3. The horizontal dynamic aperture improvement is beneficial for the beam lifetime increase, that in our case is dominated by the Touschek effect. The shown vertical aperture limit corresponds to more than 100 σ_y, with the measured coupling of the machine, and this reduction is not expected to affect the lifetime. Beam lifetime and cubic coefficient c_{11}

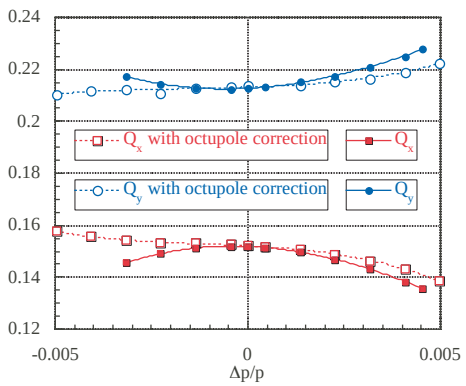

Figure 2: Measured chromaticity, with and without the octupole correction, (KLOE optics, cp progresse$^+$ ring, sextupoles on).

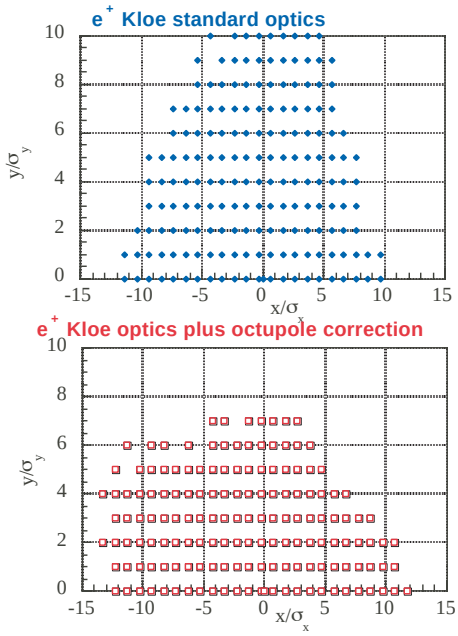

Figure 3: Above: dynamic aperture in number of sigmas of the Kloe standard optics, for positrons. Below: dynamic aperture of the same optics plus the octupole correction (σ_y full coupling, σ_x off coupling).

Table 4: Normalized beam-lifetime and c_{11} vs second order chromaticity correction (Kloe optics), with a single bunch current $I_0 \approx 10\text{mA}$, and $R_0 \approx 0.08$ at the sinchrotron light monitor.

τ_{norm} [s]	c_{11}^{meas}	applied correction [%]
1300	-77	0
1590	+15	20
1460	+80	40
1390	-	60

have been also measured: Table 4 reports the normalized beam-lifetime [8], $\tau_{norm} = \tau(\frac{I}{I_0})^{2/3}(\frac{R_0}{R})$, as a function of the applied correction, together with the measured c_{11} values. Here I is the bunch current and R the ratio of the beam sizes, $R = \frac{\sigma_y}{\sigma_x}$. The best lifetime was observed for the 20% second order chromaticity correction when the c_{11} value is reduced down to zero.

3 MEASUREMENTS IN COLLISION

In the DEAR experiment configuration, the tuning of the strength of two octupoles has been performed in collision to optimise peak luminosity, beam lifetime, and background rate. This optimisation work has been done also on the sextupole settings. A beam-lifetime increase of 15% has been obtained from the sextupole and a further 15% from the octupole optimisation. The octupoles have been found useful to improve the beam lifetime in collision because they compensate the strong beam-beam non-

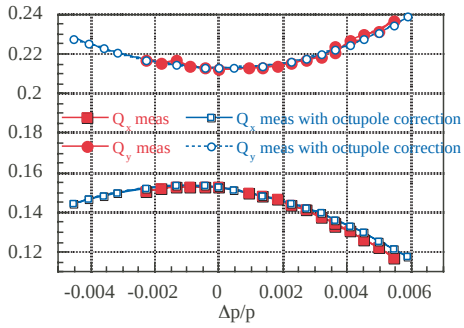

Figure 4: Measured chromaticity for the DEAR optics, e^+ ring, with and without octupole correction.

linearities. Measurements of the chromaticity, for the standard DEAR optics and for the "octupole compensated" one are shown in Fig. 4. An energy acceptance increase of the 30% is evident. Besides, the second order coefficient is reduced of about the 15% in both horizontal and vertical plane, while the cubic non-linearity, c_{11} value, is lowered from ≈ -450 down to ≈ -300.

4 CONCLUSIONS

Measurements have been performed at DAΦNE in order to study the effect of the octupole magnets installed early this year. From the first results, the benefit of using octupoles to correct both second order chromaticity and tune shift on amplitude was clear. Simulations are still in progress to improve the non linear model. This effort will be useful to predict octupole and sextupole configurations capable to enlarge the dynamic aperture and increase the beam lifetime without loss of luminosity.

5 AKNOWLEDGMENTS

The authors wish to warmly thank J.M. Jowett for his precious suggestions and helpful discussions.

6 REFERENCES

[1] G. Vignola, DAΦNE Project Team, "DAΦNE The Frascati Φ-Factory", PAC'93, Washington, May 1993.

[2] C. Milardi, et al., "Effects of nonlinear terms in the wiggler magnets at DAΦNE", PAC 2001, Chicago, June 2001.

[3] C. Sanelli, S. Han, "Design of an Octupole Magnet for DAΦNE", DAΦNE Tech. Note M-5,Frascati March 2001

[4] C. Vaccarezza, et al., "Non linear beam dynamics at DAΦNE", PAC 2001, Chicago, June 2001.

[5] A. Drago, et al., "The dynamic tracking acquisition system for DAΦNE e^+ e^- collider", DIPAC 2001, Grenoble, France, 2001.

[6] M. Preger, private communication.

[7] H. Grote and F.C. Iselin, "The MAD program (Methodical Accelerator Design)"

[8] S. Guiducci, "Beam lifetime studies at DAΦNE", these proceedings.

SIMULATIONS AND MEASUREMENTS OF THE TOUSCHEK BACKGROUND AT DAΦNE

M. Boscolo, M. Antonelli, S. Guiducci, INFN-LNF, Frascati, Italy

Abstract

DAΦNE [1] background is dominated by Touschek scattering. Many efforts have been put in its reduction, by adjusting optical parameters, and by the insertion of additional collimators. Background rate at the experiments KLOE [2] and DEAR [3] has been reduced. Effectiveness of the new collimators installed in the two rings is presented and compared with simulation showing a qualitative agreement.

Studies on the distribution and trajectories of the Touschek particles at KLOE and DEAR interaction regions (IRs) are discussed.

1 INTRODUCTION

The beam lifetime in DAΦNE and the machine induced background at the experiments are dominated by Touschek scattering: off-momentum particles can exceed the momentum acceptance of the RF bucket or may hit the aperture limit when displaced by dispersion. In addition, a betatron oscillation is excited if the momentum change takes place in a dispersive region. The reduction of this background is a challenging task in a short machine like DAΦNE.

At the beginning of data taking both experiments KLOE and DEAR suffered from large induced background. Many efforts have been put in its reduction, by adjusting optical parameters, like sextupoles strengths, orbits, β_x at the IRs, by the insertion of additional collimators in the two rings and by properly shielding the DEAR detector. The results of these optimizations show an overall background reduction at the two experiments.

During the last DEAR run (March-April 2002) the background has been reduced by a factor greater than 10.

The KLOE run has started in May 2002 and a background reduction by about a factor 3 has been obtained up to now, with respect to the last 2001 run. For example, we compare two typical days of data taking (6/12/01 and 15/05/02). The average calorimeter rates in the forward regions (endcaps), west for positrons and east for electrons, decrease from values ~130 KHz (~90 KHz) to ~40 KHz (~50 KHz) for the positron (electron) beam. The average luminosity is about the same, ranging from 3.5 to 3.2 $cm^{-2}s^{-1}$, and now the currents are ~10% lower than December.

2 SIMULATION

The home developed tracking code 'STAR' is used to predict the locations where the off-energy particles hit the vacuum chamber of the ring, with particular care at the position of the losses at the two interaction regions.

All magnetic elements are taken into account, including sextupoles and the octupolar components in the wigglers [4]. Touschek scattered particles are generated separately in the four arcs PL1, PS1, PS2 and PL2 for the positron beam (see Fig. 1). Only particles with a relative energy deviation between 0.003 and 0.02 have been considered, since particles with higher energy deviation get lost locally and do not contribute to the experimental background rate. On the other hand, particles with lower energy deviation never reach the physical aperture and do not contribute to the beam losses. The particles are tracked over many turns and those lost at the KLOE IR have been fully simulated in the detector allowing the evaluation of the background counting rates and detailed studies of background properties, namely spatial distribution and energy spectra. Several comparisons have been performed between simulations and KLOE data showing a good qualitative agreement [5] [6].

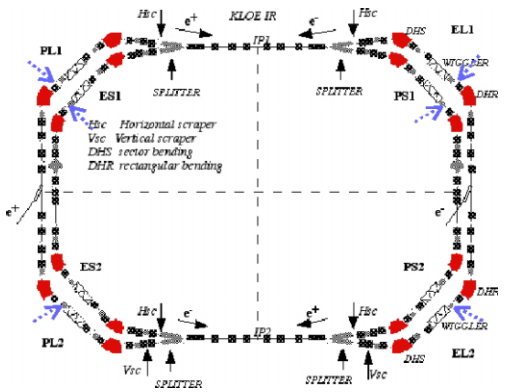

Figure 1: DAΦNE layout with old scrapers (black arrows before splitter magnets) and additional new scrapers (big blue arrows) installed in non-zero dispersion regions.

3 NEW COLLIMATORS EFFECTIVENESS

A set of movable collimators (scrapers) is used at DAΦNE to reduce the background in the detectors. These collimators are placed upstream each IR in the two rings [7]. To obtain a further background reduction three new scrapers have been installed in the arcs of each ring in January 2002 on the basis of the simulation studies [8]. The position of the new scrapers is shown in Fig. 1.

During last DEAR runs, the total background reduction at the CCDs due to the insertion of the scrapers and shielding (see Section 4.1) has been about a factor 3. The measured KLOE calorimeter rates and the positron beam lifetime are shown in Fig. 2 versus position of the inner scraper edge measured in single beam (e+) operation. The scraper opening is measured from the beam pipe edge. About 60% of background reduction is obtained.

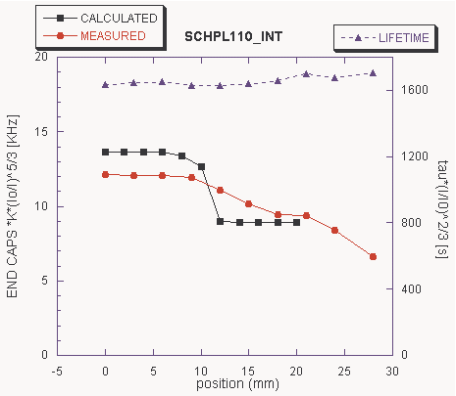

Figure 2: Scan of the background rate in the KLOE forward calorimeter versus position of the internal jaw of the scraper SCHPL110: measured (calculated) normalized rate in red dots (black squares) and normalized lifetime in blue triangles.

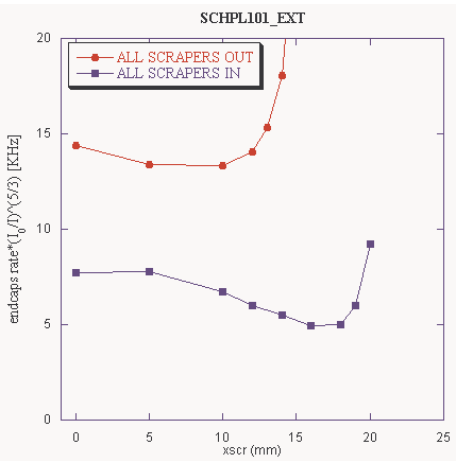

Figure 3: Scan of the normalized background rate in the KLOE forward calorimeter versus position of the external jaw of the positron beam KLOE scraper, with all other collimators out (red dots) and in (blue squares).

The normalizations of the background rate and lifetime are in accordance with the lifetime scaling law: $\tau \propto \sigma_l \sigma_x \sigma_y / I$ where σ_l is the current dependent bunch length $\sigma_l \propto I^{1/3}$ [9] and the horizontal and vertical rms beam sizes σ_x and σ_y are related by the roundness $R = \sigma_y / \sigma_x$. Therefore for a constant σ_x we have $\tau \propto R/I^{2/3}$ and the background rate $dN/dt \propto I/\tau \propto I^{5/3}/R$. Fig. 2 shows also the corresponding calculated rate, evaluated by tracking Touschek scattered particles from their origin in the arcs into the KLOE detector. The endcap acceptance has been taken into account by means of full detector simulation including the geometrical details of the IR. There is a qualitative agreement between measurement and simulation.

In addition to a direct background reduction the new collimators help in making the scrapers upstream the experiments more effective. In fact, as they are very close to the detectors, their insertion can increase background. Fig. 3 shows the efficiency of the scraper upstream KLOE with and without the other collimators inserted. A factor 1.6 is gained due to the fact that the scraper can be inserted closer to the center of the pipe. The new scrapers stop particles that would be just deviated by the IR scraper and eventually lost at the experiment. In the present KLOE running configuration the overall effectiveness of the scrapers is a factor ≈ 3 for the positron beam and ≈ 7 for the electron one. However, with the scrapers inserted, the contributions of the two beams to the endcap rates are about the same.

4 BACKGROUND AT IRS

The trajectories of the Touschek particles and their hit position along the beam pipe have been studied in the two IRs with the simulation. The background can be reduced both by properly shielding the detectors and by reducing the beam envelope where the particles are expected to be lost, i.e. by reducing the β_x-function.

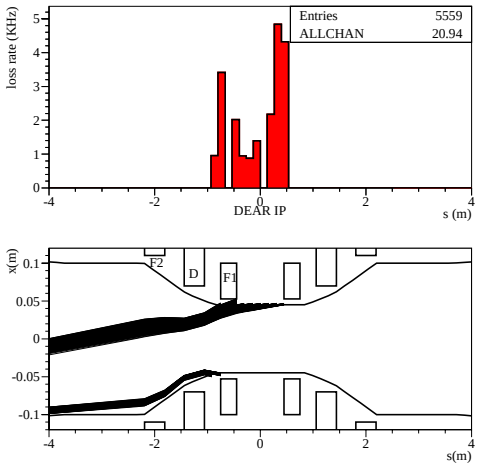

Figure 4: Distribution and trajectories of Touschek particles lost at DEAR IR, β_x (IP2) is 4 m.

4.1 DEAR Experience

The calculated trajectories and distribution of the particles hitting the pipe at the IR are shown in Fig. 4 for the optics used during the first period of data taking. Most particles are lost very close to the DEAR interaction point (IP2), and a reduction of background rate has been achieved by shielding the detector taking into account the simulation. In this particular case the shielding could be easily carried out, as DEAR consists of a small detector placed at ~15cm above the beam line. Touschek particles get lost radially but induce background vertically by scattering and shower with the beam pipe material.

The value of β_x at IP2 was reduced both to improve luminosity performance [10] and to reduce the background. In the following the effect on the background is described. It is shown in Fig. 5 the reduction of β_x at IP2 from ≈ 4.5m to ≈ 1.6m and consequently at the focusing quadrupole (QF1) close to the IP2 With this change the particles get lost at QF2 farther from IP2, as indicated in Fig. 6. These particles have been easily shielded. This optics change brought a background reduction to the experiment of about a factor 3.3.

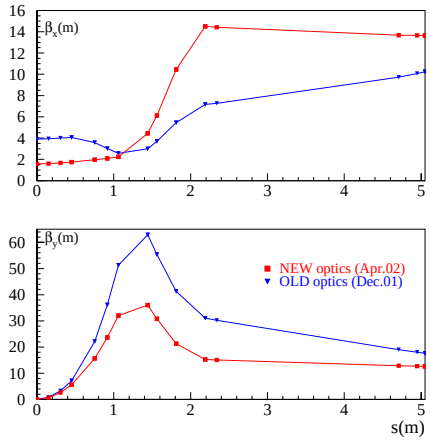

Figure 5: βx (upper) and βy (lower) function in IR2 from IP2 to splitter magnet.

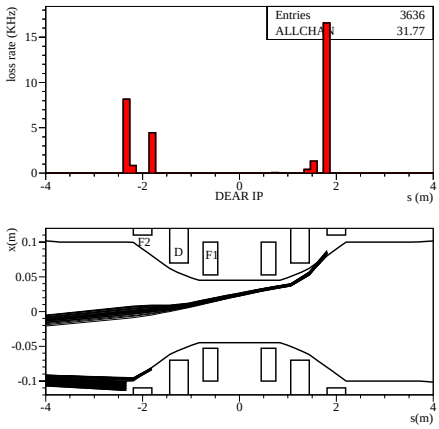

Figure 6: Distribution and trajectories of Touschek particles lost at DEAR IR, β_x (IP2) is 1.5m.

4.2 KLOE Experience

Calculated trajectories and distributions are shown in Fig. 7. Due to the different layout most of the particles are lost at the focusing quad far from IP1 (QF2) and only a small fraction at the first one close to IP1 (QF1). The distribution of this latter background component has been measured with the KLOE detector showing a good agreement with the simulation [7] [8]. Simulations indicate that the background component coming from QF2 could be reduced by a mask insertion just below the quadrupole. The mask cannot be inserted because the IR is inside the detector, therefore it will be mounted in the new IR that will be installed at the end of this year.

In fact, the installation of a new IR has been designed. As in the DEAR case the β_x will be reduced at IP1 in order to decrease the background component coming from QF1. Simulations are under way to optimize the quadrupoles and masks position for the new IR.

5 CONCLUSIONS

Measurements have been performed to investigate the new collimators performance, showing an overall decrease of the induced background rates. A qualitative agreement has been found with simulation.

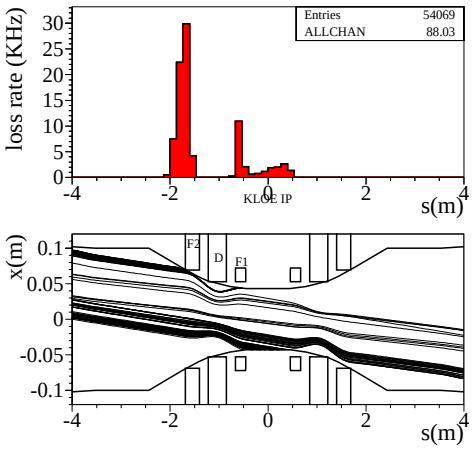

Figure 7: Distribution and trajectories of Touschek particles lost at KLOE IR with the present optics.

The new scrapers also increase the efficiency of the scraper upstream the experiments. In fact, the new collimators stop particles that would be just deviated by the IR scraper and eventually lost at the experiment.

A detailed study of the distribution of the particles hitting the pipe at the two IRs has been very useful to find the proper tools to control the background rates. In particular, the DEAR background has been reduced by a factor greater than 10 by shielding the experiment at the calculated position, by scrapers and by reducing the β_x-function at the focusing quadrupole closest to IP2. The experience gained with DEAR has been useful for the design of a new interaction region for KLOE, to be installed on DAΦNE at the end of the year, which will provide a lower β_x at the focusing quadrupole close to IP1 and shielding behind the other quadrupole farther from IP1.

6 REFERENCES

[1] G. Vignola and DAΦNE Project Team, “DAΦNE, The Frascati Φ-factory”, PAC93, Washington, 1993.

[2] The KLOE collaboration, ”The KLOE Detector, Technical Proposal”, LNF-93/002, 1993.

[3] The DEAR Collaboration, “The DEAR case”, Riv.del Nuovo Cimento, Vol.22, N11, p.1 (1999)

[4] M. Boscolo, “Effects of non linear elements on backgrounds at DAΦNE”, 23rd Adv. ICFA Workshop on high luminosity e+e- Coll., Ithaca, NY (USA), Oct. 2001.

[5] M. Boscolo S. Guiducci, “A comparison between data and simulations of the DAΦNE beam induced background in KLOE”, DAΦNE Tech.Note IR-10, Nov. 2001.

[6] M. Antonelli, L. Passalacqua, B. Sciascia, “Investigation into the physics of DAΦNE background”, KLOE Memo 260, 2001.

[7] M. Boscolo, S. Bertolucci, C. Curceanu, S. Guiducci and G.von Holtey, “Experience with beam induced backgrounds in the DAΦNE detectors”, PAC01, Chicago, June 2001.

[8] M. Boscolo and S. Guiducci, “A study on DAΦNE scrapers efficiency”, DAΦNE Technical Note IR-11, March 2002.

[9] A. Ghigo, “DAΦNE broadband impedance”, these proc.

[10] C. Biscari et al., “Half βx at IP2”, DAΦNE Techn. Note BM-9, Frascati, April 2002.

CTF3 COMPRESSOR SYSTEM

D. Alesini, C. Biscari, R. Boni, A. Clozza, G. Delle Monache, G. Di Pirro, A. Drago, A. Gallo, A. Ghigo, F. Marcellini, C. Milardi, M.A. Preger, C. Sanelli, F. Sannibale, M. Serio, F. Sgamma, A. Stecchi, A. Stella, M. Zobov, LNF-INFN, Frascati, Italy
R. Corsini, CERN, Geneva, Switzerland

Abstract

In the CTF3 complex the Linac pulse train, 1.4 μs long, is squeezed to a 140 ns train with a peak current 10 times higher (35A) by means of the bunch interlacing technique. The compressor system consists of two rings; the first (Delay Loop) multiplies the Linac bunch frequency by a factor 2, the second (Combiner Ring) by another factor 5. The lattices of the rings and transfer lines allow fine tuning of the trajectory and bunch length. The beam impedance budget is minimized to avoid energy spread growth. The layout of the rings and the intermediate transfer lines are shown. Design of special components of the rings and measurements on the prototypes are presented.

1 INTRODUCTION

CTF3 [1] is the first test for the production of RF power at 30 GHz at the nominal CLIC parameters: power of ~ 250 MW/m corresponding to an accelerating voltage of ~ 150 MV/m are the design goals. The compression system of the drive beam is the subject of this paper.

The main challenge from the beam dynamics point of view is the manipulation of the high current/low energy beam: the energy ranges between 150 and 300 MeV (factor 8–4 below CLIC), for a bunch charge of 2.3÷1 nC (factor 1÷2.3 below CLIC). The compression system consists of a Delay Loop (DL) [2], in which the current is multiplied by a factor 2, a Combiner Ring (CR) [3] which adds a factor 5, and the Transfer Lines (TL) [4] in between the Linac, the rings and the power extraction system. Fig. 1 shows the layout of the system and in Table 1 the main parameters of the rings are listed.

Table 1: CR and DL parameters

	DL	**CR**
Length [m]	42	84
Energy [MeV]	150-300	150-300
Emittance [μrad]	0.34-0.17	0.34-0.17
Bunch length (rms) [mm]	0.5-2.0	0.5-2.0
Charge/Bunch [nC]	2.3-0.5	2.3-0.5
Isochronicity: $\|R_{56}\|$	< 0.02m	<0.02 m
Total Δp/p	5 %	5 %
Path Length Tuning [mm]	± 5 mm	± 5 mm
Max. Beta H/V [m]	10.5/14.0	11.1/11.1
Max. Dispersion [m]	1.3	0.72
Phase Advance H/V	3.96/1.38	7.23/4.14
Chromaticity H/V	-6/-8	-12.0/-8.8

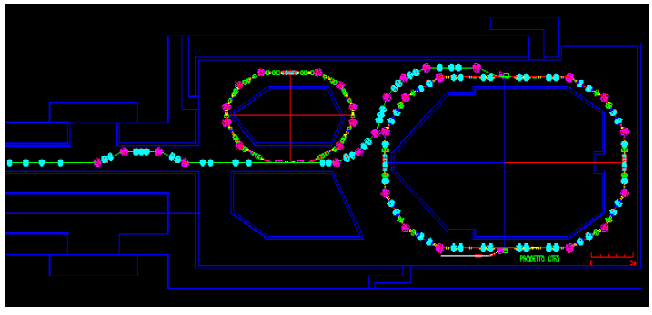

Figure 1: Compressor system layout

2 BEAM DYNAMICS

Energy losses and energy spread are of a great concern for the frequency multiplication system since they can affect strongly the efficiency of the RF power production. The energy losses give rise to relative phase errors between bunches through non-perfect ring isochronicity, which result in deterioration of the timing both between individual bunches and merging trains. The energy spread, in turn, leads to bunch lengthening and phase space distortion.

2.1 Frequency structure preservation

The power production efficiency depends on the final longitudinal beam structure at 15 GHz. Since the path followed by every bunch of each group of 10 is different, knobs to tune the path length and special care in minimizing the effects of both collective and single particle dynamics on the beam are needed.

Path length tuning devices (3-poles wigglers) are inserted in both the DL and the CR, assuring path length tunability within few mm. Adjustments with the Linac frequency on the whole train of bunches are also foreseen.

2.2 First-order beam dynamics

The bunch energy spread is affected by wake fields and by the Coherent Synchrotron Radiation (CSR). These collective effects depend on the bunch charge density and therefore on the bunch length. The latter is related to the R_{56} term of the first order transfer matrix through the energy spread and by the T_{5j6} (j=1,…6) terms of the 2nd order transfer matrix through all the 6 coordinates.

Requirements concerning bunch length variation, necessary to cope with CSR, ask for isochronicity in the rings and tunable R_{56} in the TL where all the bunches pass once. The last feature (R_{56} = ± 16 cm) is obtained by inserting a first stretcher/compressor section just after the Linac and a second one before the power extraction system.

Single particle effects can be controlled by a smooth linear optics, which makes the non-linear corrections less demanding. In the DL and in the CR fine-tuning of R_{56} by few mm is obtained by flexible optics. In the DL the isochronicity and achromaticity condition is fulfilled in each half ring, while in the CR in each quarter of the ring. The injection/extraction regions and the wigglers are placed in dispersion free sections. In the CR the optimum working point for minimum beam loading is foreseen [5].

2.3 Second-order beam dynamics

An energy acceptance of ± 2.5% is a strong requirement, especially considering that the isochronicity condition is obtained with strong horizontal focusing which makes more critical the 2nd order correction.

Second order terms relate transverse and longitudinal phase planes. In absence of sextupoles the longitudinal particle position in the bunch after going through the DL or the CR depends on the energy spread by the 2nd order term of the transport matrix, T_{566}. The minimization of this term by one sextupole family does not assure the isochronicity, since the relationship between transverse and longitudinal coordinates by the other T matrix terms produces emittance filamentation, which in turn, induces longitudinal emittance degradation. These terms are relevant for the DL and CR optics due to the small bending radius of curvature, to the high quadrupole gradients imposed by the isochronicity condition and are also influenced by the sextupoles. The contemporaneous correction of the more harming terms by three sextupole families in each isochronous section preserves the nominal beam parameters [2].

3 IMPEDANCE BUDGET AND PROTOTYPES

The experience acquired during the construction of high current colliders, like PEP II, KEKB and DAΦNE, can be successfully applied to reduce the coupling impedance of the vacuum chamber components, minimizing wake fields and CSR effects, the main sources of energy loss and energy spread [6].

The Combiner Ring impedance budget has been estimated. It has been shown that the CSR and the conventional wake fields give almost equal contributions to the energy spread and losses, which can be kept within the design limits, even for those bunches passing 5 times along the ring.

The energy spread due to CSR is $\Delta E = \pm 0.9$ MeV, or $\Delta E/E \sim \pm 0.5\%$ for a 2 mm long bunch. It is not reasonable to have bunches shorter than 2 mm in the CR since the energy spread grows rapidly with the bunch length (faster than $\sim \sigma^{-4/3}$). The energy spread for a 1 mm long bunch would exceed the acceptable value of $\Delta E/E = \pm 1\%$.

The electromagnetic design of each component of the vacuum chamber requires an accurate study aimed at reducing the impedance contribution.

The 2 RF deflectors and the 36 BPMs give the dominant contribution both to the energy spread and to the energy losses. The wake fields created by these components last longer than the distance between bunches in the trains and an additional study of the multibunch and multiturn effects is still necessary.

In the following we describe the main components of the vacuum chamber, evaluate their contribution to the impedance budget and estimate the RF energy loss and spread for the 2 mm long bunch with a charge of 2.33 nC.

3.1 RF deflectors

A pair of RF deflectors has been designed and almost completely constructed. The design procedure and the mechanical fabrication techniques are reported in ref. [7,8]. The beam dynamics in the combiner ring with the RF deflectors and, in particular, the effects of the beam loading have been carefully investigated [5].

The 2 RF deflectors give a contribution to the energy spread of 230 keV and to the energy loss of 150 keV.

3.2 Beam Position Monitor

A prototype of the Beam Position Monitor (BPM) has been built. The pickup is a transformer excited by the beam with 4 secondary windings surrounding a ferrite core placed in correspondence of a vacuum chamber ceramic gap. The beam current acts as a primary winding that drives magnetic flux in the core, inducing a voltage signal in each secondary winding with the amplitude depending on the beam position.

The pickup is designed to work in the lower end of the beam frequency spectrum, precisely in the 0.4÷100 MHz range, to reproduce only the envelope of the combiner ring bunch trains both in single and in multi-turn operation mode with 0.1 mm resolution. This sensitivity and dynamic range allow measurements with 1% of the nominal beam current.

Measurements based on the coaxial wire method have been performed in order to estimate the transfer impedance of the device, i.e. the complex ratio of the voltage induced by the beam at the external termination to the beam current (see Fig.2).

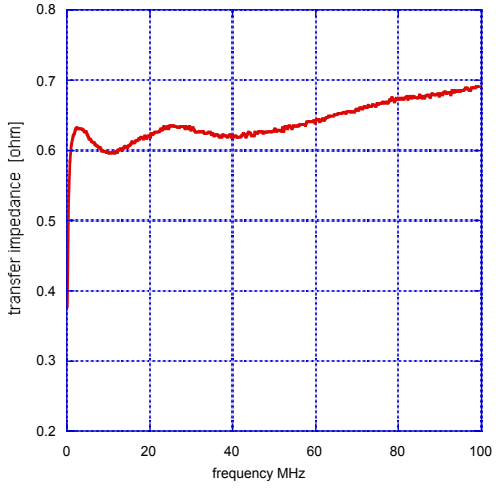

Figure 2: Transfer impedance of BPM

The overall BPM contribution to the energy spread is 330 keV. This value has been estimated from the impedance measured on similar BPMs developed at CERN. Some modification to reduce the coupling impedance is under study.

3.3 Extraction kicker

The extraction kicker has been designed with HFSS e.m. code and a first prototype has been built. A shunt impedance of 60 kΩ has been measured.

In the kicker the bunch looses 18 keV and accumulates 34 keV of energy spread after 5 turns in the CR. This contribution is negligible with respect to the previous ones.

3.4 Vacuum chamber

In the present CR vacuum chamber design the vertical dimension is kept almost constant and the number of horizontal cross section variations is reduced. Tapers are foreseen only at the arc ends, where the injection/extraction sections and the wiggler sections begin. Such a uniformity of the vacuum chamber cross section provides good vacuum conductance and allows avoiding valves.

A vacuum chamber section with a rectangular profile and with rectangular flanges has been realized. Special vacuum gaskets have been developed in order to avoid the RF contact in the junctions.

The contribution of the resistive walls can be small if the vacuum chamber is made of aluminium. The estimated losses in this case are about 12 keV, while the spread does not exceed 36 keV.

3.5 Vacuum pumps

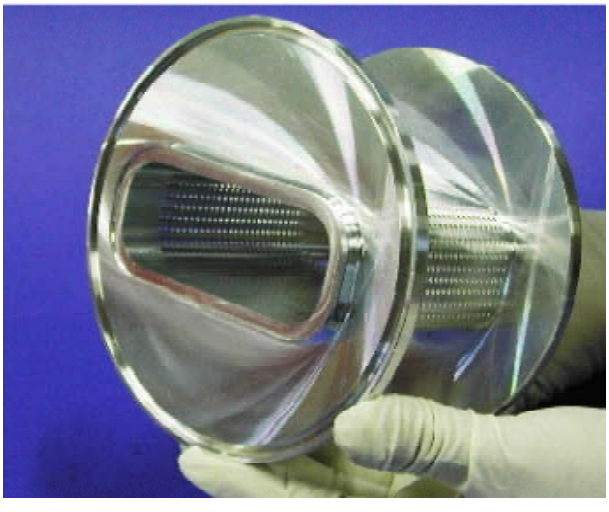

Figure 3: Vacuum pump connection

Vacuum pump connections have been realized with shielded pumping slots. The screen is composed by long grooves with hidden holes having a diameter smaller than the bunch longitudinal size. The measured conductance of a prototype section 8 cm long is 60 l/s. The section is shown in Fig. 3 before welding.

3.6 Bellows

A bellows with the RF shielding has been developed with sliding contacts having the same inner shape of the vacuum chamber. The RF shield is finger type with a minimum number of slots. Appropiate design of spring-finger assures the necessary force to maintain good electrical contact.

The inductive impedance of hidden pumping slots, sliding contact bellows, RF screened flanges are expected to be negligible.

4 CONCLUSIONS

The optics of the CTF3 compressor system has been designed with great care for first and second order beam dynamic.

A detailed analysis of the Combiner Ring vacuum chamber impedance has been done. The guidelines for the vacuum chamber design have been fixed and will be also used to design the Delay Loop and Transfer Line vacuum chamber, even though these systems are less demanding from the impedance point of view.

Prototypes of special components such as Beam Position Monitor, RF Deflectors, vacuum ports and bellows have been built and characterized.

5 REFERENCES

[1] CTF3 Design Report: http://ctf3.home.cern.ch/ctf3/CTFindex/htm.

[2] C. Biscari, “New Design for the Delay Loop in CTF3”, CTFF3-006, 2002

[3] C. Biscari, “Combiner Ring Lattice”, CTFF3-002, 2001

[4] C. Milardi, “CTF3 Transfer Line Design”, CTFF3-005, 2001

[5] D. Alesini, “The theory of beam loading in RF deflectors for CTF3”, CTFF3-007, 2002

[6] A. Ghigo, M. Zobov, “Energy Spread and Energy Losses in CTF3 Combiner Ring,” CTFF3-004, 2001.

[7] D. Alesini, “The RF Deflectors for CTF3”, CTFF3-003, 2001

[8] D. Alesini et. al “RF Beam Deflectors for CTF3 Combiner Ring”, this conference.

RF BEAM DEFLECTORS FOR CTF3 COMBINER RING

D. Alesini, R. Boni, A. Gallo, F. Marcellini, LNF-INFN, Frascati, Rome, Italy
A. Kucharczyk, S. Kulinski, M. Pachan, E. Plawski,
The Andrzej Soltan Institute for Nuclear Studies, Otwock-Swierk, Poland

Abstract

An important goal of the CLIC Test Facility CTF3 project, presently on its preliminary phase at CERN, is to verify the feasibility of bunch interlacing for the generation of 30 GHz RF power, by increasing the bunch frequency of the drive beam. Two RF deflectors are foreseen to inject in a Combiner Ring. This paper presents their design and fabrication issues.

1 INTRODUCTION

The bunch train compression scheme for CLIC test Facility CTF3 [1] relies on the feasibility of fast RF deflectors. The beam dynamics in the combiner ring and, in particular, the effects of the beam loading in the RF deflectors have been carefully investigated [2,3]. The simulation results indicate that a pair of CERN RF separators [4] (the so-called *Langeler structures*) used as RF deflectors does not degrade significantly the quality of the beam extracted from the combiner ring. The main parameters of the Langeler structure used as CTF3 RF deflectors are summarized in Table 1.

In the following we report the design procedure and the mechanical fabrication techniques followed to construct the two deflectors.

Table 1: CTF3 RF Deflector parameters.

Nom. Energy E_n	150 [MeV]
Max Energy E_{max}	300 [MeV]
Frequency f	2.99855 [GHz]
Number of cell	10
De-phasing/cell	$2\pi/3$
Cell length d	33.33 [cm]
Group velocity v_g/c	-0.0244
Phase velocity v_{ph}/c	1
RF power P_{RF}	~1.5 [MW] (@ E_n) ~6 [MW] (@ E_{max})
Deflection ϕ	5 [mrad]
$R/Q=v_g/\omega\cdot(F_\perp/e)^2/P_{RF}$	1380 [Ω/m]

2 MAFIA AND HFSS SIMULATIONS RESULTS

The design of the RF deflectors has been done scaling to the CTF3 working frequency (2.99855 GHz) the dimensions of CERN RF separators with a reduced number of cells. These are disk-loaded backward waveguides working in the $2\pi/3$ EH_{11} hybrid mode [5] already optimized [6] for beam deflection. The final 10 cells structure is sketched in Fig. 1.

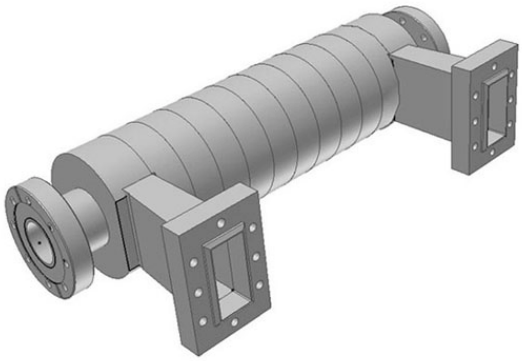

Figure 1: Sketch of the RF deflector.

2.1 Single Cell Simulations

With the electromagnetic code MAFIA [7] we have simulated the scaled single cell (Fig. 2) and we have computed the local sensitivity of the $2\pi/3$ mode frequency with respect to the variation of each cell dimension (Table 2).

Table 2: local sensitivity of the deflecting mode frequency vs. cell dimensions

Dimension	Sensitivity
a	$\partial f/\partial a$=-13.2 MHz/mm
b	$\partial f/\partial b$ =-49.7 MHz/mm
c	$\partial f/\partial t$ = 2.9 MHz/mm
d	$\partial f/\partial d$ =1.2 MHz/mm

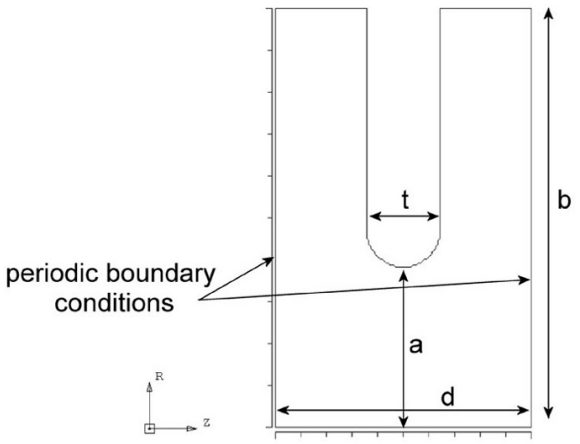

Figure 2: Sketch of the single cell 2D profile.

The $2\pi/3$ EH_{11} mode can degenerate in 2 frequencies of orthogonal polarity. The vertical one has been shifted far enough from the operating mode (horizontal polarity) in order to avoid excitation by the RF generator or the beam itself. This has been achieved by means of 2 longitudinal rods crossing off-axis the cells (just like the CERN separators) as shown in Fig. 3.

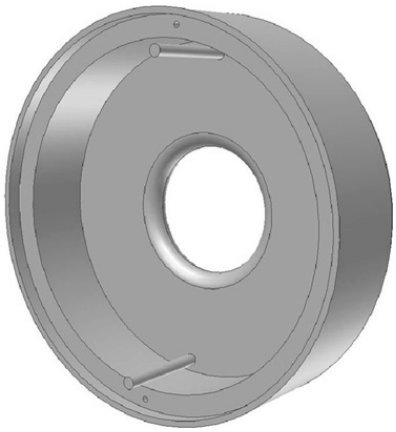

Figure 3: Sketch of the single cell 3D profile.

The frequency shift of both polarities, caused by the break of the azimuthal symmetry due to the rods, has been calculated with the code HFSS [8]. We obtained a shift of ~50 MHz for the vertical polarity and a negligible shift of the horizontal operating mode (~80 kHz).

We have, finally, calculated the $2\pi/3$ mode frequency of the single cell with rods considering also the problem of faceting in HFSS. In fact the code uses a regular polygon to model a circle or an arc and, depending on the starting vector for faceting, the polygon can be entirely inside or outside the arc to be modeled. In order to control the systematic error due to faceting, in the final single cell simulations we have considered the radius of curvature properly corrected in order to have the corresponding polygon areas equal to those of the ideal circles. The final dimensions of the single cell are reported in Table 3 with the $2\pi/3$ mode frequencies obtained by HFSS (3D cell with rods) and by MAFIA (2D cell without rods).

The dispersion curve of the deflecting mode obtained by MAFIA is plotted in Fig. 4.

Table 3: Final dimensions of the cell and RF deflectors parameters.

Final dimensions of the cells	a = 21.43 mm
	b = 56.01 mm
	d = 33.33 mm
	t = 9.53 mm
RF deflector parameters (HFSS and MAFIA)	f=2.9986 [GHz] (MAFIA) f=2.9983 [GHz] (HFSS)
	v_g=-0.0237*c (MAFIA)
	R/Q=1460 [Ω/m] (HFSS)

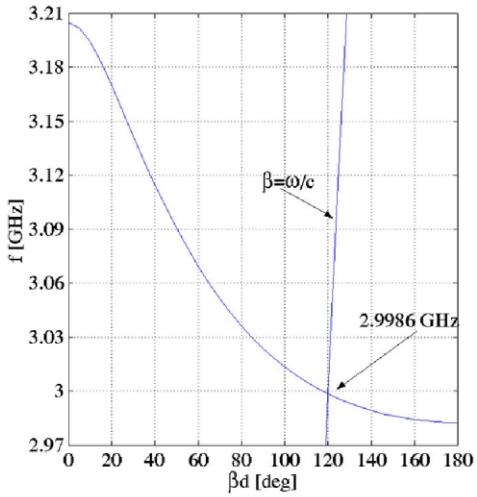

Figure 4: Dispersion curve of the deflecting mode obtained by MAFIA.

2.2 Complete Structure Simulations

In order to evaluate the coupler efficiency we have simulated with HFSS the structure with the proper boundary conditions and port excitation.

The obtained reflection coefficient (S_{11}) at the device input port is plotted versus frequency in Fig. 5. It is evident that, at the working frequency 2.99855 GHz, just few percent of the input power is reflected.

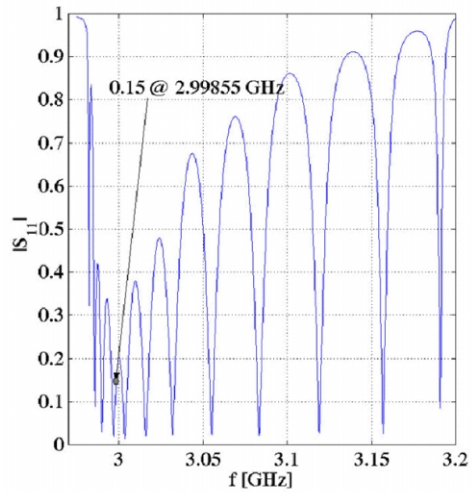

Figure 5: Reflection coefficient at the input port of the deflector as a function of frequency.

3 MECHANICAL FABRICATION TECHNIQUE

The deflectors are made of OFHC high quality copper using hard soldering (brazing) technique well mastered in production processes of accelerating structures in S band. Soldering is done in steps, in hydrogen atmosphere. Unlike the old CERN procedure, the single cells of deflector are designed and produced in the form of cups (Figure 3) reducing the number of soldered joints by a factor 2.

Before the production of the final deflectors an aluminium full-scale prototype (shown Fig. 6) has been fabricated in order to verify the validity of the performed calculations. The measurements (single cell resonant frequency, dispersion curve) have confirmed the simulation results for the two different polarities.

The deflector components are fabricated with the aid of numerical lathe and milling machines. A three steps soldering (890-780-680 °C) procedure is applied to join the deflector components. Intermediate measurements (single cell frequencies and dispersion curves before and after soldering) made on prototypes copper cells and final structures have been performed in order to control the frequencies of the cells and the changes introduced by the soldering procedure.

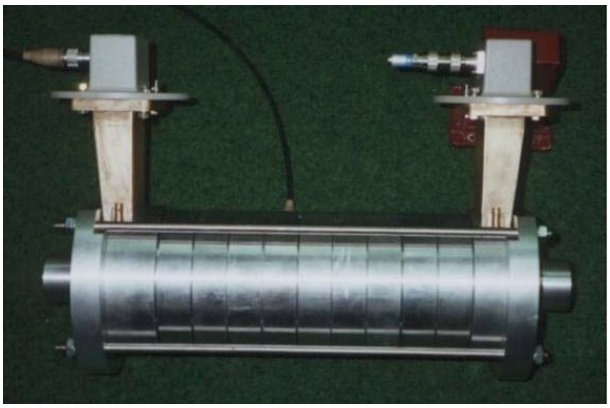

Figure 6: Aluminium prototype.

4 FINAL TUNING AND MEASUREMENTS

A dedicated test set was constructed to check the frequency of each cell before soldering. The frequencies of the first two monopoles and dipoles were measured and compared with those obtain by HFSS simulations. The frequency deviations due to the presence of measuring antennas and to the cell actual temperature were taken into account The comparison of the calculated and measured frequencies in a sample of 8 cells is reported in Table 4.

Table 4. Comparison of calculated and measured frequencies of the cells before soldering

		Mono 0	**Mono π**	**Dipole π**	**Dipole 0**
		MHz	MHz	MHz	MHz
HFSS		2105.7	2176.8	3010.9	3226.0
		Measured frequency deviation [MHz]			
Cell Number	1	-0.295	-0.674	0.096	-0.846
	2	-0.395	-0.599	-0.179	-0.846
	3	-0.325	-0.549	-0.079	-0.771
	4	-0.435	-0.675	-0.189	-0.926
	5	-0.375	-0.535	-0.264	-0.840
	6	-0.335	-0.594	-0.044	-0.826
	7	-0.335	-0.554	-0.104	-0.825
	8	-0.295	-0.534	-0.104	-0.826

The measured dispersion curve of a stack of 8 cells (+2 half cells) before soldering is shown in Fig. 7 and is in a very good agreement with the simulations results.

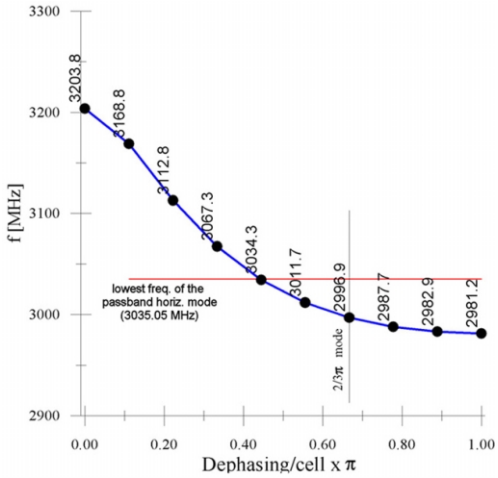

Figure 7: Dispersion curve of the defl. mode measured in air at 24.5 °C with 8 cells (+2 half cells) before soldering.

To evaluate the effect of soldering, a series of 4 pilot copper cells was measured before and after soldering. The results are shown in Table 5. Being the deflector relatively short the effect of soldering is quite negligible and, anyway, can be taken into account.

Table 5: Resonant frequencies of an assembling of 4 pilot copper cells before and after soldering.

Mode	Freq. before solder [MHz]	Freq. after solder [MHz]	Δf [kHz]
1	2986.180	2986.006	-174
2	3002.830	3002.484	-346
3	3043.374	3943.177	-197
4	3126.250	3126.030	-220
5	3211.924	3211.582	-342

5 CONCLUSIONS AND ACKNOWLEDGEMENT

The first deflector is almost ready for shipment to LNF for vacuum tests. It will be installed within June 2002 in the EPA ring for the CTF3 preliminary phase. the second deflector will be ready within July 2002. The authors warmly thank Mr. G. Fontana for the fruitful collaboration in the mechanical design of the deflectors.

6 REFERENCES

[1] H. H. Braun et al., CERN 99-06, 1999
[2] A. Gallo et al., proc. of EPAC 2000 Conf., p. 465
[3] D. Alesini et al., CTFF3-003, 2001
[4] D. Alesini, CTFF3-007, 2002
[5] Ph. Bernard et al., CERN 68-30, 1968
[6] Y. Garault, CERN 64-43, 1964
[7] Ph. Bernard et al., CERN 70-26
[8] http://www.cst.de
[9 http://www.ansoft.com/home2.cfm

BEAM DYNAMICS STUDY OF A MUON COOLING EXPERIMENT WITH 200 MHz CAVITIES IN THE FRAMEWORK OF THE CERN COOLING STUDY

M. Migliorati, L. Palumbo, Università di Roma "La Sapienza", and INFN - LNF, Frascati, Italy,
F. Tazzioli, C. Vaccarezza, INFN-LNF, Frascati, Italy
K. Hanke, E. B. Holzer, A. Lombardi, CERN, Geneva, Switzerland

Abstract

Muon cooling is one of the building blocks for a Neutrino Factory. It has the potential to increase the muon flux at the detector by an order of magnitude. Different set-ups for the experimental observation of cooling are proposed and discussed by an international collaboration [MICE]. In this paper we present the results of the tracking studies for a cooling experiment based on 200 MHz cavities with superconducting solenoids and liquid hydrogen absorbers. For 200 MeV muons passing through a system of 4 cavities at 7.6 MV/m, the number of muons in a given acceptance increases by a factor of about 10 %. This is believed to be well within capability of the measurement apparatus and sufficient to gather important information for the final design of a full-scale cooling channel.

1 INTRODUCTION

A Neutrino Factory (NF) based on a muon storage ring is an important tool for studies of neutrino oscillations. Ionization cooling of muons is fundamental for a NF, but has never been realized in practice. In the CERN layout for the NF, the cooling channel is based on 44 and 88 MHz cavities with integrated superconducting solenoids [1].

An international collaboration on a muon ionization cooling experiment (MICE) has been set up in order to study the feasibility of a section of cooling channel that would be able to give the performances required for a NF. For the CERN case, a cooling experiment has been proposed which is a small subset of the 88 MHz part of the final channel[2].

As an alternative to the cooling experiment based on 88 MHz cavities, we present a system at 200 MHz as proposed in the US study II design for a NF [3]. The aim is to verify the possibility of using cavities at 200 MHz with the same beam characteristics as in the 88 MHz case, and to compare the cooling performances in the two cases. Even with a completely different beam optics, the beam dynamics shows a similar cooling efficiency.

2 LAYOUT

The use of pill-box cavities with conductive irises resonating at 200 MHz prevents the possibility of integrating the solenoids into the cavities as in the case of 88 MHz [4].

Since a design of a cooling channel with 200 MHz cavities has already been presented in the US study II proposal [3], we have simulated a system based essentially on the same engineering constraints, but with differences due to the different beam dynamics, that in our case has characteristics similar to the 88 MHz cooling channel. In the US proposal there are two possible schemes: SFOFO lattice 1 and 2. Preliminary simulations [5] showed that, for our beam dynamics, the second scheme, with groups of two cells separated by solenoids, gives a more uniform magnetic field and better performances. We have therefore based our simulations on this set-up with the difference that we use a scheme with equal solenoid polarity. This cheap solution is not the one proposed for the full-scale cooling channel, but it can give a clear demonstration of muon cooling.

The solenoid configuration is illustrated in Fig. 1 where the magnetic field lines as computed with the POISSON code [6] are shown. In the input and output diagnostic sections there are two continuous solenoids with a radius of 33 cm and length of 2 m. At the entry of the cooling channel there is a 47 cm long liquid hydrogen absorber inserted inside a solenoid of 21 cm inner radius. The absorber is followed by a system of two cavity cells resonating at 200 MHz with an average effective gradient of about 11.8 MV/m. In the middle of the cells and outside of them there is a short solenoid (18 cm) with a large radius of 61.5 cm. After the two cells, there is another 40 cm long solenoid with an aperture of 21 cm that contributes to maintain the magnetic field as uniform as possible. The second part of the cooling channel is identical to the first, with two more cavity cells followed by the exit absorber. The total length, including diagnostics, is 8.6 m, and we have assumed a physical aperture of 20 cm. The total energy lost in the absorbers at a kinetic energy of 200 MeV corresponds to the energy gained in the cavity system.

3 BEAM DYNAMICS

The coil arrangement shown in Fig. 1 results in a longitudinal magnetic field on axis of Fig. 2 from which the PATH simulation code gives the emittance diagram of Fig. 3.

For a kinetic energy of 200 MeV and $\Delta E = \pm 30$ MeV, the final normalized rms emittance is 4630 π mm mrad, which, compared to the input emittance of 4900 π mm mrad, gives a reduction of about 5.6 % with

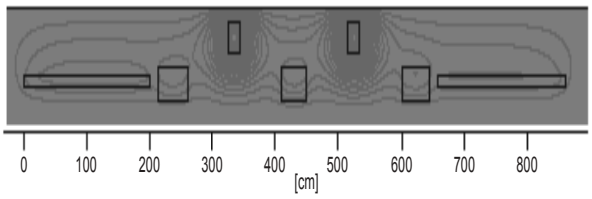

Figure 1: Solenoid layout and magnetic field lines computed with POISSON. The system has a cylindrical simmetry with respect to the horizontal axis.

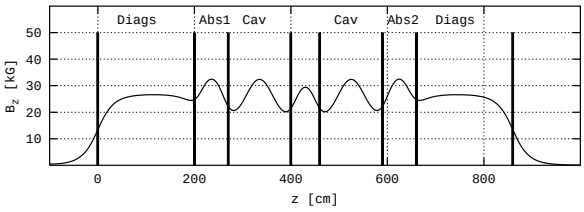

Figure 2: Longitudinal magnetic field on axis.

a particle transmission of 100 %. The initial beam parameters are $\beta_{x,y} = 1$ m, $\alpha_{x,y} = 0$, and the number of particles is $N = 50000$. The cavity system is set to work on crest. If we define the cooling efficiency as the increase of the number of particles inside a given acceptance, and use as acceptance 15000 π mm mrad (normalized) in both transverse dimensions, we get an efficiency of 8.8 %.

In Fig. 4 we show the output versus input emittance. For an input emittance of about 3000 π mm mrad (r.m.s. normalized) the equilibrium emittance is reached. Below this threshold the beam is heated. The transmission remains 100 % up to the maximum emittance that we have simulated, 10000 π mm mrad. In Fig. 5 we show the cooling efficiency, as defined above, for a range of input r.m.s. emittance. It is negative for small input emittances (heating) and goes up to about 20 % for the largest input emittance.

We have run the same set-up at input beam energies of 140 MeV and 230 MeV, adjusting slightly the solenoid field, and also in these two cases the transmission is about 100 % up to the largest input emittance.

With the scheme of the cooling channel that we have illustrated, it is possible to change the solenoid currents and work with other values of the magnetic field. For example, with the magnetic field shown in Fig. 6 (on axis), which is about a factor of 1.5 higher than the previous case, the same cooling performance is achieved even if the emittance along the channel (Fig. 7), is higher. This demonstrates the flexibility of the proposed scheme.

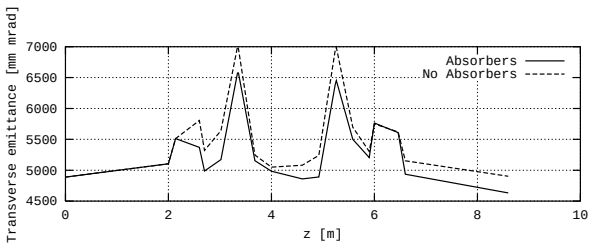

Figure 3: Transverse emittance (r.m.s., normalized) along the channel with and without absorbers.

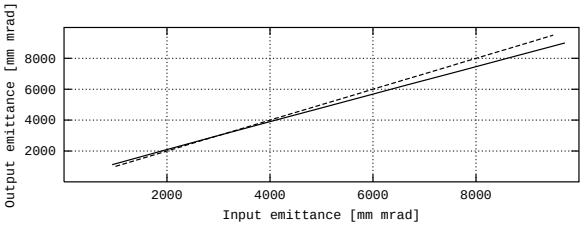

Figure 4: Output emittance vs input emittance (r.m.s., normalized) at 200 MeV.

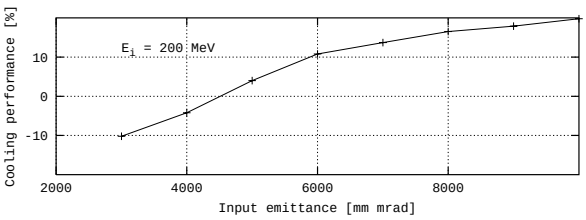

Figure 5: Cooling efficiency vs input emittance (r.m.s., normalized) for an input beam of 200 MeV.

4 FIGURE OF MERIT OF THE COOLING EXPERIMENT

In the cooling channel of the NF, the relevant figure of merit is the increase of the number of muons in the acceptance of the downstream accelerators. This acceptance is defined independently in the three planes (x, y and longitudinal). To increase the figure of merit, correlations between the planes have to be minimized at the point of transition from solenoidal focusing to quadrupole focusing.

In the cooling experiment, the emittances are measured inside the solenoid field. If the beam dynamics of the experiment is not chosen to minimize inter-plane correlations, there is no possibility to compensate for these correlations. In a general solenoidal beam transport, correlations will

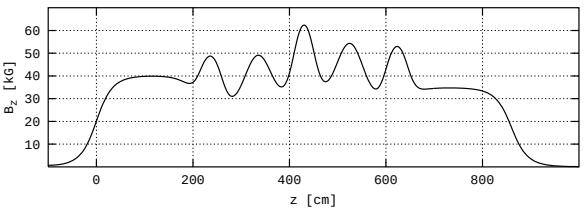

Figure 6: Alternative longitudinal magnetic field.

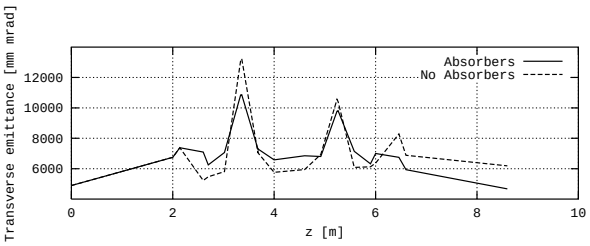

Figure 7: Transverse emittance (r.m.s., normalized) along the channel with and without absorbers for the magnetic field of Fig. 6.

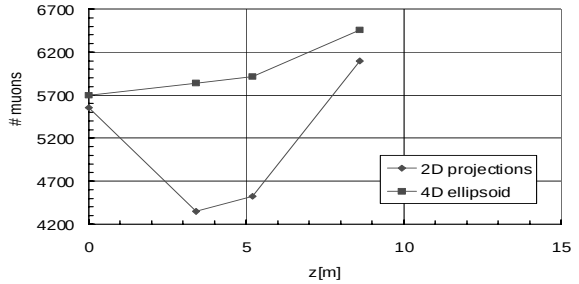

Figure 8: Number of muons inside a 4D volume of $(15000\ \pi$ mm mrad$)^2$ for a cooling experiment at 200 MHz.

mainly develop between the x and the y plane. Therefore, an algorithm was developed to count particles in 4D or 6D hyper-ellipsoids, to be used as figure of merit for the cooling experiment in the presence of inter-plane correlations [7]. It allows to measure 4D and 6D cooling rather than the 2D projections.

Fig. 8 shows the number of muons inside a normalized 4D volume of $(15000\ \pi$ mm mrad$)^2$ as a function of distance for the 200 MHz cooling experiment. Values are shown at the beginning and the end of the experiment and at two points in the middle, where $\epsilon_x \times \epsilon_y$ peaks (at 3.4 m and 5.2 m, compare to Fig. 3). The inter-plane correlations are 0, 0.7, 0.6 and 0.14 respectively at the 4 analyzed positions. At the points of high correlation, the method of 2D projections does not give a useful result for measuring the cooling performance of the experiment. The figure of merit calculated in the 4D ellipsoid and the 2D projections is 13.3% and 9.9% respectively. Counting the muons in 4D or 6D yields a stable figure of merit in the presence of correlations. The 4D ellipsoid looks at a more central core of the distribution and has therefore a higher density of muons and a slightly higher figure of merit than in the 2D projections.

5 CONCLUSIONS

We have simulated a possible scenario for a muon ionization cooling experiment at 200 MHz with the goal of comparing it from a beam dynamics point of view with the 88 MHz channel proposed at CERN. In particular, we optimized the cooling efficiency, which has to be well in the range of the proposed emittance diagnostics [8]. We find that in terms of cooling efficiency this scheme shows a performance comparable with the 88 MHz case. The set-up at 200 MHz has a naturally higher acceleration gradient which results in a better cooling rate per metre. However, the overall cooling performance of the two systems (8 cavities at 88 MHz versus 4 cavities at 200 MHz) is, as the total absorber length is the same, comparable. The choice of frequency is therefore a technical one, i.e. for a required minimum cooling efficiency one has to consider the total length of the system, number of cavities used, achievable gradient and rf power.

A major difference between the two schemes is the arrangement of the solenoids. The large bore solenoids between and around the 200 MHz cavities result in a magnetic field pattern which is less homogeneous than in the case of the 88 MHz cavities, where the solenoids (all identical) are integrated in the cavity such that they are close to the beam and generate a periodic structure. Consequently, for the 200 MHz system, the coil arrangement and hence the magnetic field along the channel vary much more. This results in strong coupling between the planes, thus giving large transverse emittance oscillations along the channel.

Another technical difference is that the 200 MHz cavities have to be separated by conducting windows in order to achieve the required gradient. This could result in unacceptable high dark current. Also, windows might break during cavity conditioning.

6 ACKNOWLEDGMENTS

This paper includes important contributions by Arnaud Perrin who passed away in a tragic accident.

7 REFERENCES

[1] A. Lombardi, 'A 40-80 MHz System for Phase Rotation and Cooling', CERN Neutrino Factory Note 37 (2000).

[2] M. Aleksa, et al., 'Beam Dynamics Study of a Muon Ionization Cooling Experiment', CERN-Nufact-Note-108 (2002).

[3] S. Ozaki, R. Palmer, M. Zisman, J. Gallardo (ed.), 'Feasibility Study-II of a Muon-Based Neutrino Source', BNL-52623 (2001).

[4] F. Tazzioli, private communication.

[5] M. Migliorati et al., 'Preliminary Study of the Cooling Channel based on the 200 MHz Cavities', presented at the Workshop on a Muon Ionization Cooling Experiment, October 25-27, 2001, CERN.

[6] J. H. Billen, L. M. Young, 'Poisson Superfish', Los Alamos National Lab report LA-UR-1834.

[7] E. B. Holzer, CERN Neutrino Factory Note 111, in preparation.

[8] P. Janot, private communication.

DESIGN STUDY OF A SOFT X-RAY SASE-FEL SOURCE

L. Palumbo on behalf of the SPARX design study group[*†‡§]

Abstract

FEL's based on SASE (Self Amplified Spontaneous Emission) effect are able to generate coherent radiation with unique features. In principle the brilliance of the source is several order of magnitudes higher than the Synchrotron Radiation Sources of third generation, and it is possible to reach the x-ray spectrum region with ultra-short pulses of hundreds femto-seconds. This source is believed to be a powerful tool to explore the frontiers of basic sciences, from physics to chemistry to biology. Intense R&D programs have started in USA and Europe, in order to understand the SASE physics and to proof the feasibility of these sources. The allocation of considerable resources in the Italian National Research Plan (PNR) brought to the formation of a CNR-ENEA-INFN-"Tor Vergata" University study group. An R&D program (SPARC Project) at LNF has been recently approved and close to start while schemes of a soft-X rays source ranging from 1.5 to 13 nm (SPARX Project) have been investigated and proposed to the Italian Government.

1 SCIENTIFIC CASE

X-rays from synchrotron light sources are today widely used in atomic physics, plasma and warm dense matter, femto-second chemistry, life science, single biological molecules and clusters, imaging/holography, micro and nano lithography. The X-rays are the ideal probe for determining the structure on the atomic and molecular scale. The big step in the peak brilliance, several orders of magnitude, expected with the FEL-SASE sources will open new frontiers of research. New techniques in X-imaging, time resolved spectroscopy can be applied in the field of material science, biology, non linear optics. Of particular relevance are the diffractive techniques with coherent radiation on biologic tissues that allow the crystallography of macro-molecules with single pulses.

2 FEL-SASE SOURCE

Two spectral complementary regions around 13.5 nm and 1 nm, are considered for the source. In order to generate the SASE-FEL at these wavelengths, it is necessary to produce a high brilliance beam to inject inside two long undulators. A preliminary analysis of the beam parameters required for such a source leads to values reported in Table 1.

Table 1: Beam parameters

Beam Energy	2.5	GeV
Peak current	2.5	kA
Emittance (average)	2	mm-mrad
Emittance (slice)	1	mm-mrad
Energy spread (correlated)	0.1	%

We envisage to use the same beam to feed two undulators whose characteristics are discussed in Table 2-3.

Table 2: Undulator characteristics (first undulator)

Undulator 1 – UM1	
Type	Halbach
Period	3 cm
K	1.67 (@ 1.5 nm)
Gap	12.67 mm (@ 1.5 nm)
Residual field	1.25 T

Table 3: Undulator characteristics (second undulator)

Undulator 2 – UM2	
Type	Halbach
Period	5 cm
K	4.88 (@ 13.5 nm)
Gap	12.16 mm (@ 13.5 nm)
Residual Field	1.25 T

As in all laser systems, the FEL-SASE signal starts from chaotic noise which is then amplified (exponential growth) and eventually saturates. Those three different phases are clearly shown in Figs. 1-2 concerning the generation of radiation at 1.5nm and 13.5nm respectively. The typical "steps" in the exponential rise are due to beam focusing regions where there are no undulators (and therefore the light beam is not amplified).

The characteristics of the FEL-SASE radiation up to the 5th harmonics, have been investigated by means of several codes: GINGER, GENESIS, MEDUSA, PROMETEO, PERSEO, and the results are shown in Table 4.

[*] D. Alesini, S. Bertolucci, M.E. Biagini, C. Biscari, R. Boni, M. Boscolo, M. Castellano, A. Clozza, G. Di Pirro, A. Drago, A. Esposito, M. Ferrario, V. Fusco, A. Gallo, A. Ghigo, S. Guiducci, M. Incurvati, P. Laurelli, C. Ligi, F. Marcellini, M. Migliorati, C. Milardi, L. Palumbo, L. Pellegrino, M. Preger, P. Raimondi, R. Ricci, C. Sanelli, F. Sgamma, B.Spataro, A. Stecchi, A. Stella, F. Tazzioli, C. Vaccarezza, M. Vescovi, V.Verzilov, C. Vicario, M. Zobov *(INFN /LNF)*; E. Acerbi, F. Alessandria, D. Barni, G. Bellomo, C. Birattari, M. Bonardi, I. Boscolo, A. Bosotti, F. Broggi, S.Cialdi, C. DeMartinis, D. Giove, C. Maroli, P. Michelato, L. Monaco, C. Pagani, V. Petrillo, P. Pierini, L. Serafini, D. Sertore, G. Volpini *(INFN /Milano)*; E. Chiadroni, G. Felici, D. Levi, M. Mastrucci, M. Mattioli, G. Medici, G. S. Petrarca *(INFN /Roma1)*; L. Catani, *(INFN /Roma2)*.

[†] R. Bartolini, F. Ciocci, G. Dattoli, A. Doria, F. Flora, G. P. Gallerano, L. Giannessi, E. Giovenale, G. Messina, L.Mezi, P.L.Ottaviani, L. Picardi, M. Quattromini, A.Renieri, C. Ronsivalle *(ENEA/FIS)*.

[‡] L.Avaldi, R.Camilloni, C.Carbone, S.Colonna, A.Cricenti, I.P.DePadova, S.Lagomarsino, C.Ottaviani, P.Perfetti, A.Pifferi, T.Prosperi, C.Quaresima, V.Rossi Albertini, N.Zema *(CNR)*.

[§] S.Stucchi, D.Flamini, C.Schaerf, A Cianchi, A.Desideri, S.Morante, S.Piccirillo, N.Rosato, V.Sessa, M.L.Terranova (*Univeristy of Rome "Tor Vergata"*)

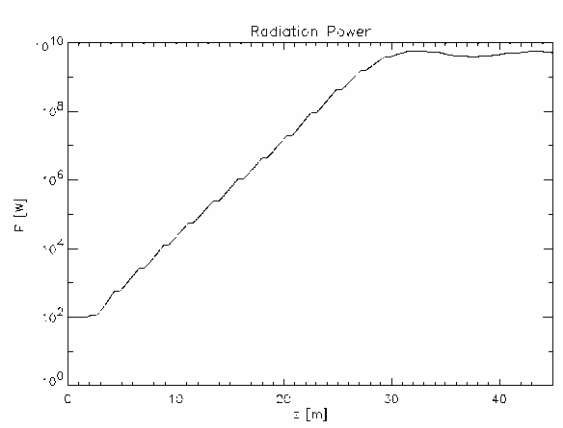

Figure 1: FEL signal evolution (λ=1.5 nm) along the undulator 1 (see Table 2).

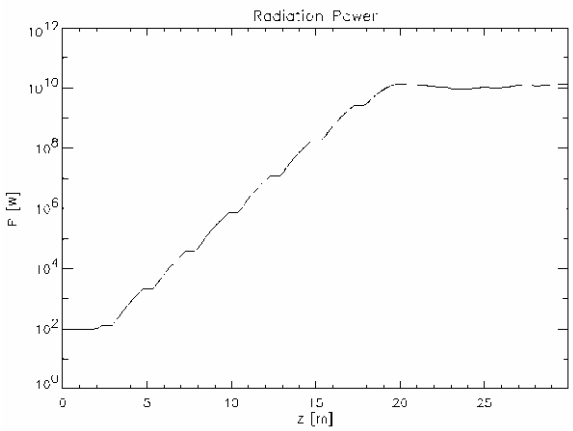

Figure 2: FEL signal evolution (λ=13.5 nm) along the undulator 2(see Table 3).

Table 4: FEL-SASE expected performances

Wavelength (λ)	1.5 nm	13.5 nm
Saturation length	24.5 m	14.5 m
Peak Power	10^{10} W	4 10^{10} W
Peak Power 3rd harm.	2 10^{8} W	5 10^{9} W
Peak Power 5th harm.	3 10^{7} W	2 10^{8} W
Brilliance**	1.8 10^{31}	2 10^{32}
Brilliance** 3rd harm.	10^{29}	10^{31}
Brilliance** 5th harm.	9 10^{28}	3 10^{29}

With the two undulators it is possible to cover a bandwidth from 1.2nm to 13.5nm, with the first harmonic, and a bandwidth from about 0.4nm to 4nm, using the 3rd harmonic, which exhibits still a considerable peak power, as shown in Fig. 3.

It is worth noting that the spontaneous synchrotron radiation power emitted by the beam inside the two undulators is (at least) two orders of magnitude higher than in the 3rd generation light sources (see for example Fig. 4).

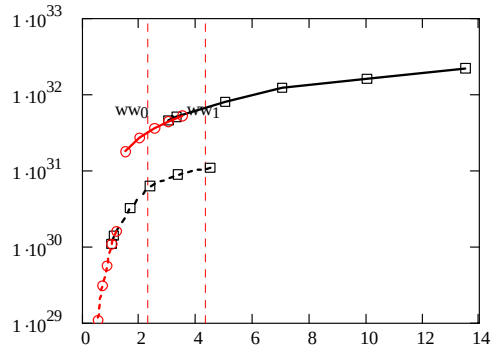

Figure 3: Brilliance** as a function of the λ (nm) at constant energy.

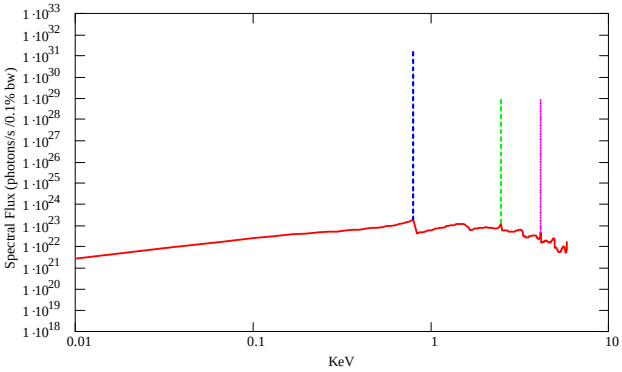

Figure 4: Spectral flux for three FEL harmonics compared to the synchrotron light contribution (see Table 2, 2.5 kA).

3. LINAC R&D AND LAY-OUT

The accelerator dedicated to the FEL-SASE source has the task of accelerating ultra-brilliant electron bunches up to the energy of 2.5 GeV. Given the charge Q in the bunch and the r.m.s. dimensions σ_x, σ_y, σ_z, the brilliance is defined as: $B_n = 2I/\varepsilon_n^2$, where $I = cQ/\sqrt{2\pi}\sigma_z$ is the peak current and $\varepsilon_n = \gamma\sigma_x\sigma_y$ the normalized emittance.

The nominal values for the proposed source are: energy E=2.5 GeV (γ=4892), peak current 2.5 kA, normalized emittance 2 μm, energy spread 0.1%. A beam with these characteristics hasn't yet been generated; however, it is believed to be achievable with the current R&D world-wide activity on photo-injectors and bunch compressor schemes.

A dedicated R&D program (SPARC project) is envisaged at LNF-INFN, in collaboration with CNR and ENEA. Its aim is the generation of electron beams with ultra-high peak brightness and the generation of resonant higher harmonics in the SASE-FEL process. The proposed scheme (Fig. 5) consists of a RF gun operated at

** The brilliance is given in photons/sec/0.1%bw/(mm mrad)^2

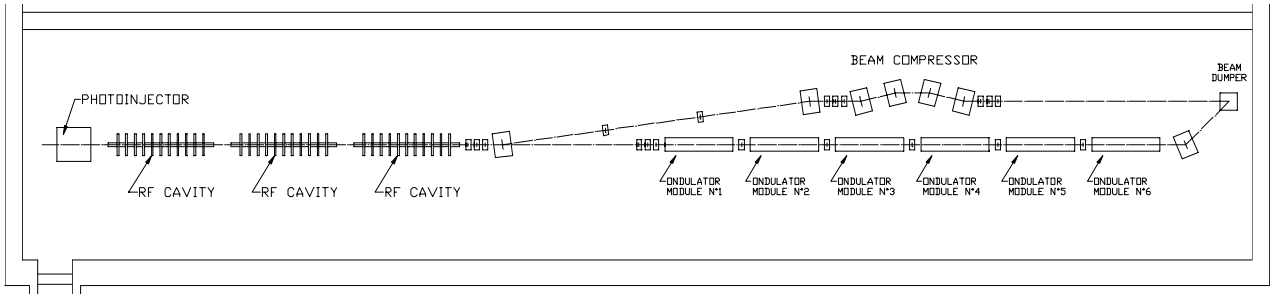

Figure 5: Schematic layout of SPARC R&D project

S-band (2.856 GHz) and high peak field on the cathode (120-140 MeV/m) with incorporated metallic photo-cathode (Copper or Mg), generating a 6 MeV beam which is properly focused and matched into 3 accelerating sections of the SLAC type (S-band, travelling wave).

The peak current will be in excess of 150-200 A and will drive a SASE-FEL experiment at 520 nm, performed with a 12m undulator following the linac. The normalised emittance and the peak beam current along the injector are shown in Fig. 6. The project has been approved by the Italian Government and expected to be founded soon.

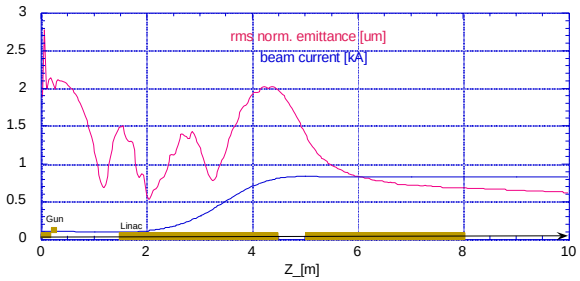

Figure 6: Beam current and normalised transverse emittance along the injector (with RF compression).

The soft X-ray project, SPARX, has been recently proposed with the schematic layout given in Fig.7. After the SPARC injector, a first 60m long accelerating section will accelerates the beam up to 1 GeV, before entering in a magnetic bunch compressor to increase the current intensity (Fig. 7). The last 90 m section will then produce the 2.5 GeV beam to be injected in the undulators. The beam parameters evolution along the whole SPARX machine is shown in Fig. 8.

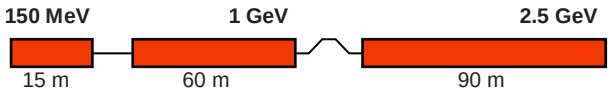

Figure 7: Linac scheme of SPARX project.

4 CONCLUSIONS

A coherent soft X ray source based on the FEL-SASE mechanism, is of great interest for many fields of applications, from basic science to industrial and medical applications. A study group gathering researchers from the major Italian research institutions (CNR, ENEA, INFN) started a conceptual design of such a source. The conceptual design was proposed to the Italian

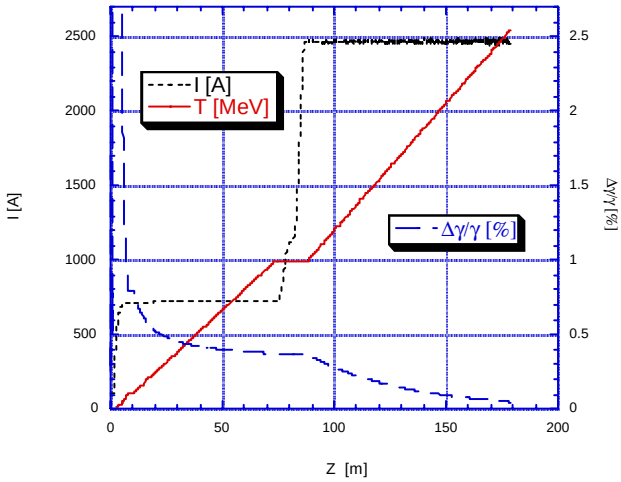

Figure 8: Beam parameters along the SPARX machine.

Government following a call for proposals issued in December 2001. The source will consist of a high brilliance photo-injector optimised for the production of very low emittance (2 μm) beams at150 MeV, and whose first accelerating section is used as RF bunch compressor,able to reach a peak current of the order of 700-800A. The R&D program for such an injector (SPARC) has already been approved and it is expected to be funded soon. After the injector, two Linacs and a magnetic compressor at 1 GeV allow a high peak current and a high quality beam, to reach the energy of 2.5 GeV. The beam is then injected into two undulators in order to generate FEL-SASE radiation (from 1.5 to 13 nm). Eventually five radiation lines bring the radiation inside an experimental area. The proposed site is the campus of the University of Rome "Tor Vergata".

5 ACKNOLEDGEMENTS

The SPARX project profits from the collaboration of many scientists worldwide. We wish to thank all the colleagues who helped us to prepare the scientific case. Concerning the source proposal, we are in debt with W.B. Fawley (LBNL), H.P. Freund (NRL), S.G. Biedron S.V. Milton (ARGONNE) and the EXOTICA international workgroup.

6 REFERENCES

[1] L. Serafini, An R&D Program for a High Brightness Electron Beam Source at LNF, this conference.

BEAM DYNAMICS STUDY OF AN RF BUNCH COMPRESSOR FOR HIGH BRIGHTNESS BEAM INJECTORS

M. Boscolo, M. Ferrario, INFN-LNF, Frascati (Roma); L. Picardi, C. Ronsivalle, ENEA, Frascati (Roma); L. Serafini, INFN-Milan, Milan

Abstract

A new method based on a rectilinear compressor scheme, utilizing the bunching properties of slow RF waves, has been recently proposed as an alternative to magnetic compressors in order to avoid beam quality degradation due to Coherent Synchrotron Radiation effects. We present here a theoretical and numerical study of the beam dynamics in an S-band photoinjector with rectilinear compressor, as proposed for the SPARC project.

1 TRANSVERSE BEAM DYNAMICS IN RADIO-FREQUENCY COMPRESSORS

Whenever a beam is injected into an RF structure at the zero acceleration phase and slips back up to the peak acceleration phase undergoing a quarter of synchrotron oscillation, it can be compressed [1].

In this section we present the theoretical description of transverse beam dynamics in RF compressors, and, in particular, the theoretical explanation on how the emittance correction process can be implemented in these devices. The analytical model is basically an extension of the invariant envelope theory [2], applicable to quasi-laminar beams carrying a constant current, to the case of currents variable along the beam line (i.e. growing together with energy along the RF compressor).

It is known that the invariant envelope is given by $\sigma_{INV} = \frac{1}{\gamma'}\sqrt{\frac{2I}{I_A\left(1+4\Omega^2\right)\gamma}}$, where the normalized beam kinetic energy is $\gamma = 1 + T/mc^2$ while the normalized accelerating gradient is defined by $\gamma = \gamma_0 + \gamma' z$ and $\gamma' \equiv \frac{E_{acc}}{mc^2}$, I is the beam peak current in the bunch, and the normalized focusing gradient is $\Omega^2 = \left(\frac{eB_{sol}}{mc\gamma'}\right)^2 + \begin{cases} \approx 1/8\ SW \\ \approx 0\ TW \end{cases}$ for a superposition of magnetic field of solenoids and RF ponderomotive focusing by Standing Wave or Traveling Wave sections. σ_{INV} is an exact analytical solution of the rms envelope equation for laminar beams

$$\sigma'' + \sigma'\frac{\gamma'}{\gamma} + \sigma\frac{\Omega^2\gamma'^2}{\gamma^2} - \frac{I}{2I_A\sigma\gamma^3} = \frac{\varepsilon_{n,sl}^2}{\sigma^3\gamma^2} \approx 0$$

where the emittance term (r.h.s.) is considered negligible (this is true in standard photo-injectors up to relevant energies, higher than 100 MeV): it corresponds to an equilibrium beam condition that assures emittance correction, i.e. a control of emittance oscillations associated to envelope oscillations such that the final emittance at the photoinjector exit is reduced to an absolute minimum. In order to assure this condition is necessary to match two types of flow along the photoinjector: the invariant envelope inside accelerating sections and Brillouin flow, given by $\sigma_{BRI} = \frac{mc}{eB_{sol}}\sqrt{\frac{I}{2I_A\gamma}}$, in intermediate drift spaces.

This analysis is valid only for beams carrying constant peak current I , as usual in photoinjectors when no compression mechanism is applied (or space charge debunching is negligible). In order to extend the model to the case of RF compression (where I grows by large factors) we have assumed that the current grows in the compressor at the same rate as the energy, i.e. $I = \frac{I_0\gamma}{\gamma_0}$, where I_0 and γ_0 are the initial values for the current and the energy, respectively, at injection into the compressor. This assumption is derived by observations performed in several simulations of the RF compressor, indicating that best results in terms of final beam brightness are achieved under this condition of adiabaticity, which indeed gives rise to a new beam equilibrium.

In fact, the rms envelope equation becomes in this case:

$$\sigma'' + \sigma'\frac{\gamma'}{\gamma} + \sigma\frac{\Omega^2\gamma'^2}{\gamma^2} - \frac{I_0}{2I_A\sigma\gamma_0\gamma^2} = 0$$

whose new exact analytical solution is $\sigma_{RFC} = \frac{1}{\Omega\gamma'}\sqrt{\frac{I_0}{2I_A\gamma_0}}$, i.e. a beam flow at constant envelope (instead of $1/\sqrt{\gamma}$ as for the invariant envelope). This is dictated by a new equilibrium between the space charge defocusing term (decreasing now as $1/\gamma^2$) and the focusing and acceleration terms (imparting restoring forces to the beam): while for the invariant envelope equilibrium is achieved even in absence of external focusing , i.e. at $\Omega = 0$, in this case we need to provide external focusing.

Just for sake of comparison we notice that the solution for Brillouin flow (i.e. drifting beam at constant energy and constant current undergoing a rigid rotation in the solenoid field B_{sol}) becomes $\sigma_{BRI}^{BAC} = \frac{mc}{eB_0}\sqrt{\frac{I_0}{2I_A\gamma_0}}$ in the case of current increasing linearly along the drift ($I = (\mu z)I_0$) for a corresponding growing solenoid field

of the type $B_{sol} = \sqrt{\mu z} B_0$ (also in this case we obtain a constant envelope matched beam through the system, like for the case of RF compression). σ_{BRI}^{BAC} describes what typically happens in ballistic bunching to the beam envelope, which needs to be taken under control by providing a ramped solenoid field to avoid envelope instability.

What is relevant for the emittance correction process is the behavior of the envelope and associated emittance oscillations due to envelope mismatches at injection: let us assume that the injecting envelope is mismatched with respect to the equilibriuum condition such that $\delta\sigma_{INV0} = \sigma_{INV} - \sigma_0$, or $\delta\sigma_{RFC0} = \sigma_{RFC} - \sigma_0$, or $\delta\sigma_{BRI0}^{BAC} = \sigma_{BRI}^{BAC} - \sigma_0$, depending on the type of equilibrium flow that the beam has to be matched on. A perturbative linear analysis of the rms envelope equations reported above (together with $\sigma'' + \sigma\left(\frac{eB_0\sqrt{\mu z}}{mc\gamma_0}\right)^2 - \frac{(\mu z) I_0}{2 I_A \sigma \gamma_0^3} = 0$ for the ballistic bunching case) brings to these solutions for the evelope mismatches:

$$\delta\sigma_{INV} = \delta\sigma_{INV0} \cos\left[\sqrt{1/4 + 2\Omega^2}\, \ln\left(\frac{\gamma}{\gamma_0}\right) + \psi_0\right]$$

for the invariant envelope,

$$\delta\sigma_{RFC} = \delta\sigma_{RFC0} \cos\left[\Omega \ln\left(\frac{\gamma}{\gamma_0}\right) + \psi_0\right]$$

for its generalization in RF compressors, and

$$\delta\sigma_{BRI}^{BAC} = \delta\sigma_{BRI0}^{BAC} \cos\left[\left(\frac{eB_0\sqrt{\mu z}}{mc\gamma}\right) z + \psi_0\right]$$

for the ballistic bunching case.

These envelope mismatches produce emittance oscillations in laminar beams because of the spread in initial mismatches due to different slice currents [2]. The emittance behaviors for the three flow conditions come out to be

$$\varepsilon_n^{INV}(z) \approx \sqrt{\varepsilon_{off}^2 + \frac{I\left\langle \delta\sigma_{INV}^2 \right\rangle}{\left(\frac{1}{4} + \Omega^2\right)\gamma'^2 \gamma}}$$

$$\varepsilon_n^{RFC}(z) \approx \sqrt{\varepsilon_{off}^2 + \frac{I_0\left\langle \delta\sigma_{RFC}^2 \right\rangle}{\Omega^2 \gamma'^2 \gamma_0}}$$

$$\varepsilon_n^{BAC}(z) \propto \sqrt{\varepsilon_{off}^2 + \frac{I_0\left\langle \delta\sigma_{BRI0}^{BAC\,2} \cos^2\left[\left(\frac{eB_0\sqrt{\mu z}}{mc\gamma}\right) z + \psi_0\right]\right\rangle}{B_0^2 \gamma_0}}$$

where the average $\left\langle \delta\sigma^2 \right\rangle$ is performed over the initial spread of mismatches in different bunch slices and ε_{off} accounts for the non linear and thermal contributions.

While the rms normalized emittance oscillates and adiabatically damps as $1/\sqrt{\gamma}$ in the invariant envelope case (ε_n^{INV}, constant current), it oscillates at constant amplitude along the RF compressor (ε_n^{RFC}), and with a frequency scaling like the invariant envelope case, i.e. $\frac{\Omega}{z}\ln\left(1 + \frac{\gamma' z}{\gamma_0}\right)$ compared to $\frac{\sqrt{1/4 + 2\Omega^2}}{z}\ln\left(1 + \frac{\gamma' z}{\gamma_0}\right)$. In the case of ballistic bunching the emittance ε_n^{BAC} exhibits on the other hand a completely different scaling, with constant amplitude but an increasing frequency like $\left(\frac{eB_0\sqrt{\mu z}}{mc\gamma}\right)$. This the basis why the transverse emittance can be corrected succesfully in the RF compressor: by connecting the two types of flow carefully (proper matching) we can make the emittance oscillates at constant amplitude in the RF compressor and connect adiabatically these oscillations to a damped oscillatory behavior in the accelerating sections following the RF compressor, where the beam is propagated under invariant envelope conditions - this is possible because of the similar frequency behavior of the two flows. It seems hardly achievable in the ballistic bunching, where the increase of the emittance oscillation frequency prevents a good matching to the invariant envelope regime, and induces the onset of non-linear space charge effects that prevent the emittance oscillations to be fully reversible (each minimum in the oscillations is slightly larger than the previous ones).

2 AN RF COMPRESSOR FOR SPARC

The SPARC [3] design assumes a 1.6-cell S-band RF gun of the same type of the BNL-UCLA one equipped with an emittance compensating solenoid and followed by three standard SLAC 3-m TW each one embedded in a solenoid. The preliminary results of the first simulations show that with a proper setting of accelerating sections phase and solenoids strength it is possible, applying the compression method described above, to increase the peak current preserving the beam transverse emittance. An optimized parameters set is shown in table 1.

In order to get a slow bunching of the beam (the current grows about at the same rate of the energy) and to increase the focusing magnetic field with the current during the compression process, we used the first two sections as compressor stages.

Table 1: RF compressor parameters

TW Section	**I**	**II**	**III**
Gradient (MV/m)	15	25	25
Phase (Deg)	-88.5	-64.3	0 (on crest)
Solenoid field (Gauss)	1120	1400	0

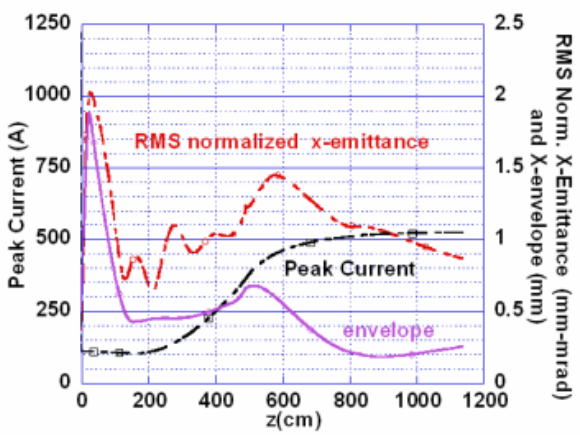

Figure 1: RMS normalized emittance, beam envelope and peak current vs the distance from the cathode.

The plots in fig. 1 of the peak current and the transverse normalized rms emittance (a thermal emittance of 0.3 mm mrad is included) as a function of the distance from the cathode computed by PARMELA for 10K particles show that a peak current of 510 A can be reached with a transverse rms normalized emittance of 0.9 mm mrad. The final beam energy is 120 MeV. The plots of figures 2 and 3 show the evolution of the bunch during the compression as derived from PARMELA computations. One can see that the bunch temporal distribution that is uniform at the beginning tends to a triangular shape: so the value of the peak current in the plot of fig.1, that is simply scaled with the rms bunch length, in reality is an average current in the bunch corresponding to a larger value in the peak (almost doubled respect to the average).

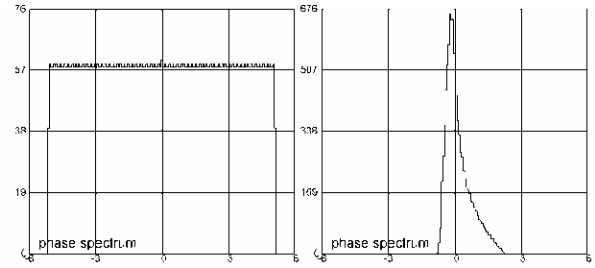

Figure 2: initial and final phase spectrum.

From the point of view of the beam transverse dynamics, during the compression slices with different longitudinal position within the bunch undergo different focusing strengths: in particular the head of the bunch which contains the maximum charge is defocused, while the tail tends to be focused or overfocused, as it shown in figure 3 which shows the plot x-phi in different points of the compressor line.
According to PARMELA convention in the plots of figure 3 and figure 4 the head of the bunch is on the left.

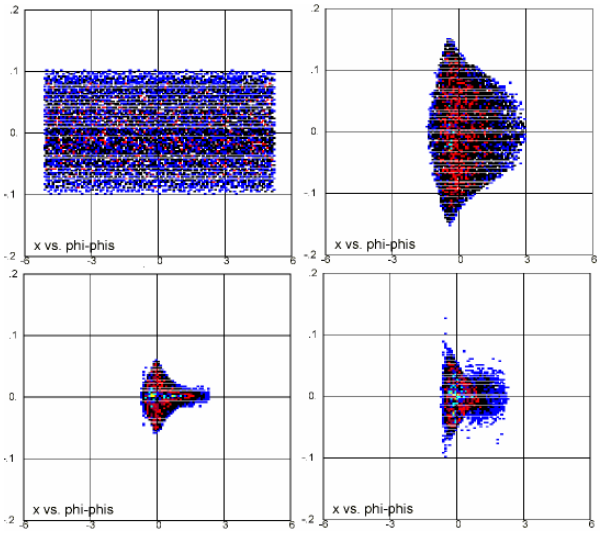

Figure 3: x-phi plot Top: left plot: initial RF gun, right plot: output Section 1, Bottom: right plot: output Section 2, left plot: output Section 3.

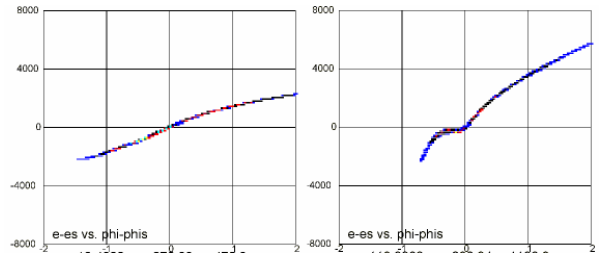

Figure 4: Energy-phase space: left: output Section 1 I=330 A, left: output Section 3 I=510 A.

From the point of view of the longitudinal phase space, as it can be seen in Figure 4, when the current becomes greater than 400 A the bunch head tends to loose the energy-phase correlation differently from the tail that contains less charge, which could be a problem for a further compression of the bunch at higher energy. This point will be investigated more carefully in the future.

3 REFERENCES

[1] L. Serafini, A. Bacci, M. Ferrario , "Ultra-short electron bunch generation with a rectilinear compressor," PAC2001, Chicago, June 2001.
[2] L.Serafini,J.Rosenzweig,*Phys. Rev. E* **55**(1997) 7565
[3] The SPARC study group, "An R&D Program for a High Brightness Electron Beam Source at LNF", These proceedings

AN R&D PROGRAM FOR A HIGH BRIGHTNESS ELECTRON BEAM SOURCE AT LNF

D. Alesini, S. Bertolucci, M.E. Biagini, C. Biscari, R. Boni, M. Boscolo, M. Castellano, A. Clozza, G. Di Pirro, A. Drago, A. Esposito, M. Ferrario, V. Fusco, A. Gallo, A. Ghigo, S. Guiducci, M. Incurvati, P. Laurelli, C. Ligi, F. Marcellini, M. Migliorati, C. Milardi, L. Palumbo, L. Pellegrino, M. Preger, P. Raimondi, R. Ricci, C. Sanelli, F. Sgamma, B. Spataro, A. Stecchi, A. Stella, F. Tazzioli, C. Vaccarezza, M. Vescovi, V. Verzilov, C. Vicario, M. Zobov *(INFN/LNF)*;

F. Alessandria, G. Bellomo, I. Boscolo, F. Broggi, S. Cialdi, C. DeMartinis, D. Giove, C. Maroli, V. Petrillo, L. Serafini, *(INFN/Milano)*;

E. Chiadroni, G. Felici, D. Levi, M. Mastrucci, M. Mattioli, G. Medici, G. S. Petrarca *(INFN /Roma1)*;

L. Catani, A. Cianchi, A. D'Angelo, R. Di Salvo, A. Fantini, D. Moricciani, C. Schaerf, *(INFN /Roma2);*

R. Bartolini, F. Ciocci, G. Dattoli, A. Doria, F. Flora, G. P. Gallerano, L. Giannessi, E. Giovenale, G. Messina, L. Mezi, P.L. Ottaviani, L.Picardi, M. Quattromini, A. Renieri, C. Ronsivalle *(ENEA/FIS);*

L. Avaldi, C. Carbone, A. Cricenti, A. Pifferi, P. Perfetti, T. Prosperi, V. Rossi Albertini, C. Quaresima, N. Zema *(CNR)*

Abstract

The design of a high gradient S-band Photo-Injector system for the production and study of high brightness electron beams is in progress at the Frascati Laboratory, in the frame of a collaboration among INFN, ENEA, CNR, Univ. Roma TV, INFM and ST. This collaboration submitted last year a proposal to a dedicated call for proposals launched by our government, meant to be the first step of a R&D program strategically oriented to a large X-ray FEL initiative. This proposal was approved (December 2001), among others, for a total allocated budget of 9.5 M€ .The construction of the system is expected to start soon: it is comprised of a RF gun driven by a Ti:Sa laser to produce 10 ps flat-top pulses on the photocathode (up to a few nC bunch charge), injecting into two SLAC structures which boost the beam up to 150 MeV. We foresee to conduct investigations on the emittance correction technique and on the RF compression (velocity bunching) scheme, which is expected to increase the natural peak current (100 A) achievable at the gun exit up to a few kA level, with proper preservation of the transverse emittance. Although the system is expected to drive a FEL experiment in the UV region, it will be used also to investigate beam physics issues like surface roughness induced wake-fields, bunch length measurements in the sub-ps range, emittance degradation in magnetic compressors due to CSR and an eventual experiment of Compton backscattering to produce sub-ps X-ray pulses.

1 ORIGIN OF THE PROPOSAL

Driven by the large interest that 4th generation light sources, i.e. X-ray SASE FEL's, have raised world-wide in the synchrotron light scientific community, as well as in the particle accelerator community, and following solicitations arising from several Italian national research institutions, the Italian Government launched in 2001 a long-term initiative devoted to the realisation in Italy of a large scale ultra-brilliant and coherent X-ray source. The initiative was modulated into two phases, with anticipated budgets of 11 M€ and 96 M€ respectively: the first phase is meant to be a 3 year R&D program strategically oriented to explore the feasibility and the most crucial issues of the system which is expected to be designed and built in the second phase, aimed at the construction of the source in a 5-6 year time scale. To pursue this program, the Italian Government published two calls for proposals, in March 2001 and in December 2001 for the two phases respectively. In March 2002 the proposal SPARC, here described, was approved, among others, to be funded with 9.5 M€ over the available total budget of the first phase (11 M€): funding should be delivered soon, allowing a prompt start-up of the project. In the meanwhile, two proposals, submitted in February 2002 at the second phase of the call for proposals, are waiting a final decision of approval: one of these, SPARX, is tightly correlated to the approved project SPARC and is presented somewhere else at this conference[1].

SPARX has been submitted by a collaboration CNR-ENEA-INFN-Univ. Roma TV.

2 THE SPARC PROJECT

The overall SPARC project consists of 4 main lines of activity aiming at several goals: their common denominator is to explore the scientific and technological issues that set up the most crucial challenges on the way to the realisation of a SASE-FEL based X-ray source. These are:

1) Advanced Photo-Injector at 150 MeV

Since the performances of X-ray SASE-FEL's are critically dependent on the peak brightness of the electron beam delivered at the undulator entrance, we want to investigate two main issues - generation of the electron beam and bunch compression via magnetic and/or RF velocity bunching - by means of an advanced system delivering 150 MeV electrons, the minimum energy to avoid further emittance dilutions due to time-dependent space charge effects [2].

2) SASE-FEL Visible-VUV Experiment

In order to investigate the problems related to matching the beam into an undulator and keeping it well aligned to the radiation beam, as well as the generation of non-linear coherent higher harmonics, we want to perform a SASE FEL experiment with the 150 MeV beam, using a segmented undulator with additional strong focusing, to observe FEL radiation at 500 nm and below.

3) X-ray Optics/Monochromators

The X-ray FEL radiation will provide unique radiation beams to users in terms of peak brightness and pulse time duration (100 fs), posing at the same time severe challenges to the optics necessary to guide and handle such radiation. This project will pursue also a vigorous R&D activity on the analysis of radiaton-matter interactions in the spectral range typical of SASE X-ray FEL's (from 0.1 to 10 nm), as well as the design of new optics and monochromators compatible with these beams.

4) Soft X-ray table-top Source

In order to test these optics and to start the R&D on applications, the project will undertake an upgrade of the presently operated table-top source of X-rays at INFM-Politecnico Milano, delivering 10^7 soft X-ray photons in 10-20 fs pulses by means of high harmonic generation in a gas. This will be a very useful bench-test for the activities performed in item 3 above.

In the following, the lay-out and planned activities for items 1 and 2 will be presented in more details, being these more related to the particle accelerator field.

3 ADVANCED PHOTO-INJECTOR

Two are the main goals of this activity in the context of the SPARC project: acquiring an expertise in the construction, commissioning and characterisation of an advanced photo-injector system (which is today missing in the Italian particle accelerator community) and performing an experimental investigation of two theoretical predictions that have been recently conceived and presented by members of this study group. These are: the so-called Ferrario's working point[2] for high brightness RF photo-injectors and the velocity bunching technique to apply RF bunch compression[3] through the photo-injector, with emittance preservation.

The 150 MeV injector will be built inside an available bunker of the Frascati INFN National Laboratories: the general lay-out of the system is shown in Figure 1.

The proposed system to be built consists of: a 1.6 cell RF gun operated at S-band (2.856 GHz, of the BNL/UCLA/SLAC type [4]) and high peak field on the cathode (120-140 MeV/m) with incorporated metallic photo- cathode (Copper or Mg), generating a 6 MeV beam which is properly focused and matched into 2 accelerating sections of the SLAC type (S-band, travelling wave).

Our simulations using PARMELA indicate that we can generate with this system a beam like that needed by the FEL experiment at 150 MeV: in Figure 2 we report the longitudinal phase space distribution at the Linac exit. The rms correlated energy spread over the bunch is 0.14% with a rms normalized emittance of 1.2 mm·mrad (at 1.6 nC bunch charge, 150 peak current), but the slice energy spread, calculated over a 300 μm slice length (comparable to the anticipated slippage length), is well below 0.05 % all over the bunch.

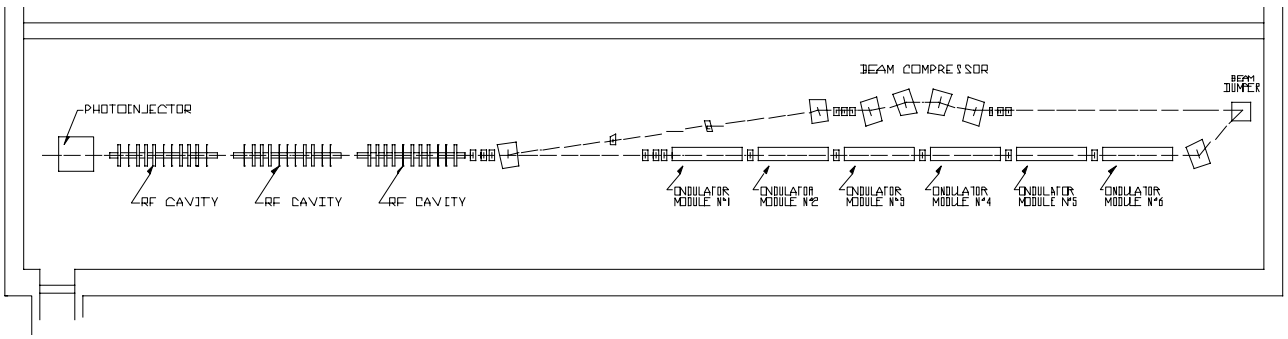

Figure 1 : Lay-out of the SPARC system.

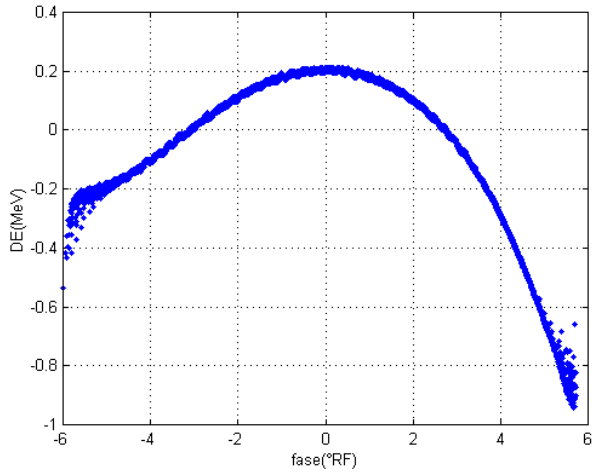

Figure 2: Longitudinal phase space distribution at Linac exit.

4 SASE-FEL EXPERIMENT

This will be conducted using a permanent magnet undulator made of 6 sections, each 2.5 m long, separated by 0.3 m gaps hosting single quadrupoles which focus in the horizontal plane. The undulator period is set at 3.3 cm, with an undulator parameter k_w= 1.88.

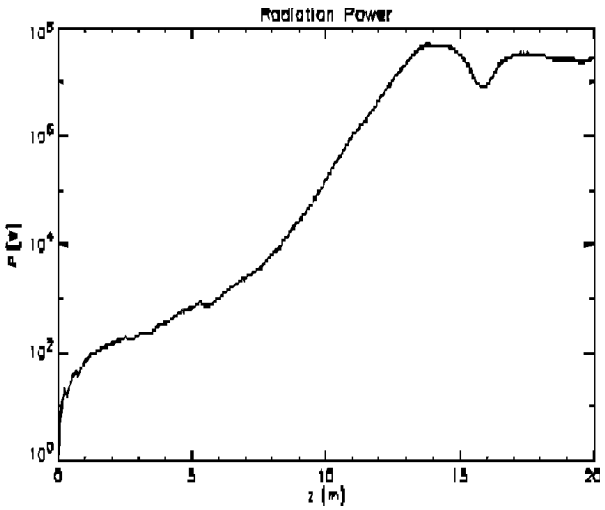

Figure 3 : Radiation Power growth along the undulator.

A simulation performed with GENESIS is reported in Figure 3, showing the exponential growth of the radiation power along the undulator: almost 10^8 Watts can be reached after 14 m of total undulator length, on the fundamental harmonic at 530 nm. Preliminary evaluations of the radiation power generated into the non-linear coherent odd higher harmonics show that 10^7 and $7x10^5$ W can be reached on the third and fifth harmonics, respectively.

5 FURTHER EXPERIMENTS

As shown in Figure 1, the SPARC lay-out anticipates two main upgrades that will be implemented in a second phase of the project: a third accelerating section which will be actually inserted between the RF gun and the 2 previous sections, and a parallel beam line containing a magnetic compressor.

The new section will be designed to study RF compression: it will support travelling waves at an adjustable phase velocity (from v=c down to v=0.999c) in order to exploit the full potentialities of the velocity bunching technique [3]. Its design and construction will proceed in parallel to the commissioning of the SPARC injector system (RF gun + 2 standard SLAC-type 3 m sections). These tests of RF compression assume great relevance in our R&D program[5] since the general lay-out for SPARX foresees the use of a mixed compression scheme, RF compression in the photoinjector up to 700 A and one single stage of magnetic compression at 1 GeV up to the final peak current of 2.5 kA.

The second beam line will allow to conduct experiments on magnetic compression: we want to experimentally investigate CSR induced effects on emittance degradation and surface roughness wake-field effects, without interfering with the ongoing FEL experiment.

6 REFERENCES

[1] D. Alesini et al., Study of a Soft X-Ray SASE-FEL Source, this conference

[2] M. Ferrario et al., Homdyn Study for the LCLS RF Photoinjector , in The Physics of High Brightness Beams, J.Rosenzweig and L.Serafini ed., World Sci., ISBN 981-02-4422-3, June 2000

[3] L. Serafini and M. Ferrario, Velocity Bunching in PhotoInjectors , AIP CP 581, 2001, pag.87

[4] D.T. Palmer, The next generation photoinjector , PhD. Thesis, Stanford University

[5] M. Boscolo et al., Beam Dynamics Study of RF Bunch Compressors for High Brightness Beam Injectors , this conference.